4. RESULTS

4.1. Main results

4.1.1. Active fork breakage and religation mediate replication restart upon transcription-replication collisions

Nagaraja Chappidi[1], Ralph Zellweger[1], Shruti Menon[1], Antonio Porro[1], Jana Dobrovolna[2], Massimo Lopes[1] and Pavel Janscak[1, 2,*,¶]

[1]Institute of Molecular Cancer Research, University of Zurich, Winterthurerstrasse 190, 8057 Zurich, Switzerland; [2]Institute of Molecular Genetics, Academy of Sciences of the Czech Republic, Videnska 1083, 143 00 Prague, Czech Republic.

*Correspondence: pjanscak@imcr.uzh.ch

¶ Lead Contact

I designed the research together with P.J. and performed majority of the experiments. I and P.J. analyzed the data and wrote the manuscript. Electron microscopy experiments were performed in collaboration with R.Z. and M.L. S.M and J.D. generated inducible U2OS T-REx stable cell line expressing wild-type RNase H1 tagged with GFP

Active fork breakage and religation mediate replication restart upon transcription-replication collisions

Nagaraja Chappidi[1], Ralph Zellweger[1], Shruti Menon[1], Antonio Porro[1], Jana Dobrovolna[2], Massimo Lopes[1] and Pavel Janscak[1,2,*,¶]

[1]Institute of Molecular Cancer Research, University of Zurich, Winterthurerstrasse 190, 8057 Zurich, Switzerland; [2]Institute of Molecular Genetics, Academy of Sciences of the Czech Republic, Videnska 1083, 143 00 Prague, Czech Republic.

*Correspondence: pjanscak@imcr.uzh.ch

¶ Lead Contact

Running title: Resolution of transcription-replication collisions

SUMMARY

Transcription-replication collisions (TRCs) mediated by co-transcriptional R-loops underlie oncogene-induced replication stress, a driver of genomic instability and tumorigenesis. Here, we demonstrate that replication fork stalling by R-loops is an active process involving RAD51-mediated fork reversal, which restrains MUS81-dependent restart of semiconservative DNA replication. Replication restart is triggered by RECQ5 helicase, which disrupts RAD51 filaments on stalled forks to counteract fork reversal and facilitate fork cleavage by MUS81/EME1 endonuclease. This relieves topological constraints generated by the convergent movement of transcription and replication machineries, allowing reactivation of transcription and subsequent replication restart, with the latter depending on the action of the single-strand annealing factor RAD52 and the DNA ligase 4/XRCC4 complex. Consistently, transcription elongation inhibitors impair replication restart upon R-loop-mediated TRCs, leading to persistence of DNA breaks. We propose that this fork breakage/religation cycle allows for TRC resolution without disruption of transcription complexes.

KEYWORDS

Replication stress, transcription-replication collision, R-loops, replication fork reversal, MUS81, DNA ligase 4, replication restart.

INTRODUCTION

During genome duplication, DNA replication forks frequently encounter active transcription complexes that can halt their progression. Such interference constitutes a major natural source of genomic instability, a hallmark of precancerous lesions and cancer cells [77]. Transcription-replication collisions (TRCs) can occur in both co-directional and head-on orientation, with the latter scenario having much stronger deleterious effect on replication fork progression and genomic integrity than the former [75, 181]. Although DNA replication is significantly co-oriented with transcription in the human genome [120], the frequency of TRCs in head-on orientation can be enhanced by deregulation of origin firing [75], which can occur upon activation of oncogenes [71, 182].

Recent studies have shown that head-on TRCs promote the formation of co-transcriptional R-loops, which represent a potent block to replication fork progression [75, 83]. These structures are generated by invasion of the nascent transcript into the DNA duplex behind the RNA polymerase (RNAP) complex, leading to the formation of an RNA:DNA

hybrid between the transcript and the template DNA strand [99]. Formation of R-loops is facilitated by negative DNA supercoiling generated behind the elongating RNAP complex and occurs preferentially in the transcriptional units containing a high G density in the non-template strand [99]. Interestingly, transcription complexes can halt the progression of converging replication forks only if the transcription unit is prone to form an R-loop, thus implying R-loops as the major cause of replication stalling induced by head-on transcription [75].

Although there is a great deal of knowledge about the strategies that cells evolved to overcome TRCs or to remove R-loops [78, 95], understanding whether and how a replication fork blocked by an R-loop can restart DNA synthesis remains elusive. Recent studies have shown that S-phase progression in cells exposed to oncogene-induced replication stress requires proteins involved in the restarting of stalled replication forks, namely MUS81 endonuclease, SLX4 scaffold protein, RAD52 strand-annealing protein and the non-catalytic subunit of DNA polymerase δ, POLD3 [161, 183-185]. The same set of proteins is also required for mitotic DNA synthesis (MiDAS) induced by stalled replication forks at common fragile sites (CFSs) to prevent chromosome mis-segregation and non-disjunction [165, 166]. As R-loop formation underlies oncogene-induced replication stress and is the cause of the instability of CFSs [71, 114], it is likely that MUS81, SLX4, RAD52 and POLD3 constitute a pathway that promotes replication fork progression through regions of active transcription.

Stalled replication forks are frequently converted into four-way junction structures resembling a chicken foot [156, 186]. This DNA transaction, termed replication fork reversal, requires RAD51 and the DNA translocases ZRANB3 and SMARCAL1, and is believed to protect stalled replication forks from being processed into DNA double-strand breaks (DSBs) [155, 156, 187]. Interestingly, recent studies have revealed that reversed forks are entry point for nascent strand degradation observed in BRCA2-defective cells upon replication arrest [154, 157, 184, 187]. These findings suggest that, while dispensable for RAD51-mediated fork reversal, BRCA2 promotes assembly of a stable RAD51 filament on the regressed arm of reversed forks to protect them from nucleolytic degradation [157, 184].

Here, we provide evidence that replication fork stalling caused by co-transcriptional R-loops is an active process involving replication fork stabilization by RAD51-mediated fork reversal. This DNA transaction is counteracted by RECQ5 helicase that disrupts RAD51 nucleoprotein filaments on stalled replication forks to facilitate MUS81-dependent replication restart. Our data suggest that the RECQ5-assisted cleavage of stalled replication forks by MUS81 endonuclease relieves the topological constraints generated by converging

transcription and replication machineries, allowing reactivation of transcription and subsequent replication restart, which involves fork religation mediated by a concerted action of RAD52 and the DNA ligase 4 (LIG4)/XRCC4 complex.

RESULTS

Replication fork stalling at co-transcriptional R-loops is an active process involving RAD51-mediated fork reversal

To study the fate of replication forks upon encounter of an R-loop, we used a well-established DNA-fiber assay, which involves labeling replication tracts with halogenated thymidine analogues followed by their visualization on DNA fiber spreads through indirect immunofluorescence. Evidence suggests that G-quadruplex (G4) structures formed in the non-template DNA strand within an R-loop enhance R-loop stability [99, 188]. We therefore sought to examine replication fork progression upon stabilization G4 structures in the cell with pyridostatin (PDS), a well-known G4-DNA-binding ligand [189]. Human osteosarcoma U2OS cells were pulsed with the first thymidine analogue CldU followed by treatment with PDS and concomitant labeling with the second thymidine analogue, IdU (Figure 1A). We observed for individual forks that IdU tracts were shorter than CldU under these conditions (Figure 1A and 1B), indicating that PDS induces replication fork slowing. Importantly, replication fork slowing in PDS-treated cells was fully rescued by inhibition of transcription with cordycepin or by overexpression of human RNase H1 (Figure 1A and 1B), which degrades the RNA strand in a RNA:DNA hybrid and thereby eliminates R-loops [99]. Thus, these data suggest that PDS slows down replication fork progression by promoting the formation of co-transcriptional R-loops.

To induce the formation of R-loops, we also used camptothecin (CPT), an inhibitor of DNA topoisomerase I (TOP1), which suppresses R-loop formation [93]. In agreement with published data [190], we observed that CPT induced replication fork slowing in U2OS cells in a manner dependent on transcription (Figure 1A and 1B). Moreover, the replication fork slowing phenotype in CPT-treated cells could be fully rescued by overexpression of RNase H1 (Figure 1A and 1B), confirming that CPT inhibits DNA replication by promoting R-loop formation. Consistently, the lengths of replication tracts of sister replication forks displayed a marked asymmetry upon CPT treatment (Figure 1C). Similar phenotype was also observed in PDS-treated cells (Figure 1C). Importantly, the sister fork asymmetry in CPT- and PDS-treated cells was fully suppressed by cordycepin or RNase H1 overexpression (Figure 1C).

CPT-induced replication fork slowing is known to be associated with RAD51-mediated replication fork reversal [156, 186], which is antagonized by poly (ADP-ribose) polymerase (PARP)-regulated replication restart, dependent on RECQ1 DNA helicase [160]. Thus, it appears that replication fork stalling caused by R-loops is an active process. In support of this notion, we found that not only CPT- but also PDS-induced replication fork slowing was rescued by PARP inhibition with olaparib or by RAD51 depletion (Figure 1D), suggesting that replication fork stalling at R-loops is dependent on fork reversal. Consistently, inhibition of transcription or over-expression of RNase H1 suppressed replication fork reversal induced by CPT or PDS treatment (Figure 1E and 1F; Table S1A).

Taken together, these results demonstrate that replication fork stalling upon encounter of co-transcriptional R-loops is an active process involving RAD51-mediated fork reversal.

Restart of replication forks stalled by co-transcriptional R-loops is mediated by the SLX4-MUS81-RAD52-POLD3 axis

Restart of stalled replication forks at CFSs in early mitosis requires MUS81/EME1 endonuclease, SLX4, RAD52 and POLD3 [165, 166]. As replication stalling at CFSs is likely to be a consequence of R-loop-mediated TRCs [114], we reasoned that these proteins might also promote the restart of R-loop-stalled replication forks in S-phase. In support of our hypothesis, we found that depletion of either of the aforementioned proteins enhanced the inhibitory effect of CPT and PDS on replication fork progression in U2OS cells and abolished the rescue obtained upon concomitant PARP inhibition (Figure 2A, 2B and S1A). Depletion of these proteins also restored the inhibitory effect of CPT and PDS on replication fork progression in cells lacking RAD51 (Figure S1B). Moreover, MUS81 depletion markedly enhanced sister fork asymmetry in CPT- and PDS-treated cells and prevented the rescue of this phenotype by PARP inhibition (Figure S1C). To further prove that the SLX4-MUS81-RAD52-POLD3 pathway operates in cells capable of fork reversal, we evaluated the effect of depletion of these proteins on replication fork velocity in U2OS cells recovering from CPT or PDS treatments. The latter were added to cells during the first pulse labeling with CldU followed by IdU labeling in absence replication-interfering drugs (Figure 2C and S1D). By measuring the lengths of IdU tracts of replication forks initiated prior to CldU labeling, we found that MUS81, SLX4, EME1, RAD52 and POLD3 were required for efficient DNA replication in cells recovering from CPT or PDS treatment (Figure 2D and S1E). On the contrary, RAD51, BRCA1 or BRCA2 were dispensable (Figure 2D, S1E and S1F), excluding a primary role of the homologous recombination machinery in the replication

restart process. Depletion of MUS81, EME1 or SLX4 did not significantly affect the replication fork velocity in untreated cells (Figure S1G).

Taken together, these data support a model wherein stalled replication forks, initially stabilized by RAD51-mediated fork reversal, are subsequently channeled into a replication restart pathway mediated by MUS81/EME1 endonuclease, RAD52 and POLD3.

RECQ5 helicase mediates the switch from active fork stalling to replication restart

Our recent studies have shown that MiDAS is promoted by RECQ5 helicase that disrupts RAD51 filaments on stalled replication forks at CFSs to facilitate fork cleavage by MUS81/EME1 endonuclease [191]. This prompted us to test whether RECQ5 is also required for restart of replication forks stalled by R-loops during S-phase. We found that RECQ5 depletion in U2OS cells compromised the rescue of CPT- and PDS-induced replication fork slowing by PARP inhibition as well as the restoration of efficient DNA replication during recovery after CPT and PDS treatments (Figure 2B, 2E, S2A and S2B). On the contrary, RECQ5 was dispensable for the rescue of CPT- and PDS-induced replication fork slowing by RAD51 depletion (Figure 2E and S2A). Similar results were obtained if cells were depleted of RECQ1 (Figure 2B, 2E, S2A and S2B), which eliminates the regressed arm of reversed forks by promoting branch migration [160]. Thus, these data suggest a model for replication restart in which RECQ5 disrupts RAD51 filaments on stalled forks to prevent fork reversal.

To further test the above model, U2OS cells were depleted of ZRANB3, which mediates fork reversal [155]. As previously reported [155], we observed that ZRANB3 depletion rescued CPT-induced replication fork slowing in these cells (Figure 2E and S2C). The same effect was observed upon PDS treatment (Figure S2A). Importantly, the rescue of replication fork slowing phenotype in ZRANB3-depleted cell was abolished be co-depletion of RECQ5, but not RECQ1 (Figure 2E, S2A and S2C). These data not only confirm that RECQ1 promotes replication restart by converting reversed forks to the original three-way structure, but also provide evidence that RECQ5 eliminates RAD51 filaments assembled on stalled forks prior to fork reversal. Consistently, depletion of RECQ5 as well as depletion of the subunits of the MUS81 endonuclease complex enhanced the level of fork reversal both in untreated and CPT-treated cells (Figure 2F; Table S1B). Moreover, cells expressing RECQ5 mutants defective in disrupting RAD51 filaments, namely RECQ5K58R and RECQ5F666A [191], displayed an elevated frequency reversed forks and a defect in replication restart upon CPT treatment (Figure S2D-S2F). Co-depletion of RECQ5 and MUS81 or MUS81 and SLX4 increased fork reversal frequency to levels comparable with those observed upon depletion of

either protein alone, confirming that RECQ5, MUS81 and SLX4 act in a common pathway that counteracts fork reversal (Figure 2F).

Taken together, these data suggest that RECQ1 and RECQ5 regulate the balance between replication fork reversal and restart at sites of R-loop-mediated TRCs.

RECQ5-assisted cleavage of stalled forks by MUS81/EME1 endonuclease mediates replication restart upon TRCs

Having identified the factors required for restarting replication forks stalled by R-loops, we next aimed to elucidate the underlying molecular mechanism. Inhibition of PARP activity in CPT-treated cells leads not only to the restoration of replication fork progression, but it is also associated with accumulation of DSBs [186]. By pulsed-field gel electrophoresis (PFGE), we could observe that PARP inhibition stimulated DSB formation not only in CPT-treated but also in PDS-treated U2OS cells (Figure 3A). Moreover, we found that DSB accumulation under these conditions was suppressed by inhibition of DNA replication or transcription, or by overexpression of RNase H1 (Figure 3A), suggesting that DSBs form as a consequence of R-loop-mediated TRCs and might represent an intermediate in the process of TRC resolution. Most importantly, we found that depletion of MUS81 or EME1 as well as depletion of SLX4, which binds and activates MUS81/EME1 for replication fork cleavage on the leading arm [192], prevented accumulation of DSBs in CPT- and PDS-treated cells upon PARP inhibition (Figure 3B and S3A). Moreover, accumulation of DSBs under these conditions was suppressed in cells depleted of RECQ5 (Figure 3B and S3A) or cells expressing RECQ5 mutants defective in disrupting RAD51 filaments (Figure S3B and S3C), providing further evidence that RECQ5 stimulates replication fork cleavage by MUS81/EME1 *via* disruption of RAD51 filaments.

MUS81 binds to SLX4 through a conserved motif, termed the SAP domain, which is located at the C-terminus of SLX4 [193, 194]. Formation of the MUS81/SLX4 complex is dramatically enhanced upon entry into mitosis through phosphorylation of the SAP domain by CDK1 [195, 196], and SLX4 is required for the recruitment of MUS81/EME1 to sites of persistent replication intermediates in mitotic prophase [166]. However, we found that DSB accumulation in CPT- and PDS-treated cells was not impaired upon inhibition of CDK1 with RO3306 (Figure S3D and S3E), suggesting that these DSBs are generated by SLX4-associated MUS81 endonuclease prior to entry into mitosis. Consistently, we found that PARP inhibition did not cause accumulation of DSBs upon CPT treatment and did not rescue CPT- and PDS-induced replication fork slowing in a FA-P-patient-derived (SLX4 deficiency)

cell line complemented with SLX4 ΔSAP cDNA [194] (Figure 3C and 3D). Of note, SLX4 mutants lacking the SAP domain also failed to rescue the sensitivity of these cells to CPT [194].

To further prove that MUS81 endonuclease acts at sites of R-loop-mediated TRCs during S-phase, we analyzed the nuclear distribution of MUS81 in U2OS cells prior to and after treatment with CPT or PDS. We found that both CPT and PDS treatments stimulated the formation of MUS81 nuclear foci that co-localized with FANCD2 foci (Figure 3E and 3F), suggesting that MUS81 accumulates at stalled replication forks. Importantly, the formation of MUS81 and FANCD2 foci in CPT- or PDS-treated cells was impaired by transcription inhibition or by RNase H1 overexpression (Figure 3G, 3H and S3F), implying dependence on R-loop-mediated TRCs. Moreover, MUS81 foci formation in CPT-treated U2OS cells was impaired by SLX4 depletion (Figure 3I and S3G), suggesting that MUS81 recruitment to stalled replication forks is mediated by SLX4. Depletion of EME1 also abrogated MUS81 foci formation in CPT-treated (Figure 3I and S3H), confirming that MUS81 acts at R-loop-stalled replication forks as part of the MUS81/EME1 heterodimer.

Collectively, these data suggests that restart of replication forks stalled by R-loops is initiated through RECQ5-assisted cleavage of the leading arm by MUS81/EME1 endonuclease in complex with SLX4.

Replication restart upon R-loop-mediated TRCs occurs *via* replication fork reestablishment

The finding of POLD3 as a factor required for replication stress-induced DNA synthesis was interpreted as the involvement of break-induced replication (BIR) [161, 166], where newly synthesized DNA strands segregate with the broken chromatid [197]. However, APH-induced MiDAS as well as the restart of CPT- and PDS-stalled replication forks during S-phase are independent of RAD51 [165] (Figure 2D), which is essential for BIR-mediated restart of collapsed replication forks in yeast [198]. Moreover, our analysis of EdU incorporation patterns on metaphase chromosome spreads indicated that MiDAS predominantly occurred on both sister chromatids, indicative of a semiconservative mode of DNA replication (Figure 4A-4C and S4A-S6E). To assess whether the DNA synthesis initiated after replication fork stalling at R-loops during S-phase also occurs in a semiconservative manner, we tested whether the nascent DNA strands generated in BRCA2-defective upon CPT treatment are sensitive to nucleolytic degradation if DNA replication is blocked by hydroxyurea (HU) [158]. We reasoned that this would indicate that replication

restart at R-loops occurs *via* replication fork reestablishment as the degradation of nascent DNA strands in BRCA2-deficient cells is initiated by fork reversal [157, 184]. Replication tracts in BRCA2-depleted U2OS cells were sequentially pulse-labeled by CldU and IdU, with CPT added during the second labeling. This was followed by HU treatment for 5 h (Figure 4D). To prevent nascent strand degradation during CPT treatment, cells were simultaneously treated with olaparib, which blocks fork reversal [157]. The same analysis was performed with RAD51-depleted cells that are also resistant to blockage of DNA synthesis by CPT or PDS, but are defective in fork reversal [154, 156, 157]. As expected in cases of semiconservative DNA replication, we found that upon HU treatment, IdU tracts were degraded in BRCA2-depleted cells, but not in RAD51-depleted cells (Figure 4D). Importantly, the extent of HU-induced nascent strand degradation in BRCA2-depleted cells pretreated with CPT and PARPi was comparable to that measured in cells treated with HU only (Figure 4D), excluding the possibility that nascent strand degradation occurred only at the forks that were not impaired by R-loops. Essentially the same results were obtained if CPT was substituted with PDS (Figure S4F). Nucleolytic degradation of nascent DNA strands could also occur during BIR if HU-induced replication arrest resulted in D-loop disruption. If this is the case, however, IdU tract shortening should be detectable in both BRCA2- and RAD51-depleted cells, which was not observed in our experiments (Figure 4D and S4F). Thus, these data provide support for the model where MUS81 endonuclease promotes the restart of semiconservative DNA replication upon R-loop-mediated TRCs.

Replication restart upon R-loop-mediated TRCs depends on RAD52 and LIG4/XRCC4 activities

We considered the possibility that the restoration of replication fork after its cleavage by MUS81/EME1 endonuclease occurred *via* RAD52-mediated re-annealing of the parental strands. In this case, replication restart would be dependent on the activity of a DNA ligase able to seal the nick in the leading strand template. To test this hypothesis, we depleted U2OS cells of either DNA ligase 3 (LIG3) or DNA ligase 4 (LIG4) and evaluated whether the absence of these proteins impairs the rescue of CPT- and PDS-induced replication fork slowing by PARP inhibition with olaparib. We found that the olaparib-stimulated replication fork progression in CPT- and PDS-treated cells was abolished upon depletion of LIG4, but not LIG3 (Figure 5A and S5A). DNA synthesis under these conditions also required XRCC4 (Figure 5A and S5A), which forms a complex with LIG4 and stimulates its activity [199]. On the contrary, KU70 was dispensable (Figure 5A), excluding the involvement of the non-

homologous end-joining machinery in replication fork restart. LIG4 and XRCC4, but not LIG3 or KU70, were also required for efficient DNA replication upon CPT or PDS removal (Figure 5B), and their depletion further reduced replication fork velocity in cells treated with CPT or PDS in absence of olaparib (Figure 5A and 5C). Moreover, co-depletion of LIG4 with RAD52 reduced DNA synthesis in CPT- or PDS-treated cells to levels comparable to those observed in cells depleted only for either LIG4 or RAD52 (Figure 5A), suggesting that these two proteins operate in a common replication fork restart pathway. Consistently, we also found that cells depleted of RAD52 or LIG4 displayed elevated levels of MUS81-dependent DSBs upon treatment with CPT (Figure 5D).

To assess whether the catalytic activity of LIG4 was required for the rescue of replication fork progression in CPT- or PDS-treated cells by PARP inhibition, we used hTERT-immortalized fibroblasts derived from a LIG4 syndrome patient (411BR) carrying a hypomorphic homozygous mutation (R278H) in the catalytic domain of LIG4, which reduces the adenylation and ligation activities of the enzyme to 5-10% of wild-type activity [200, 201]. The 411BR patient has also two additional amino acid substitutions (A3V + T9I) at LIG4 N-terminus (A3V+T9I) that further reduce the polyadenylation and ligation activity of the R278H mutant without impacting LIG4 protein levels or interaction with XRCC4 [200-202]. By DNA fiber assay, we found that PARP inhibition did not rescue CPT- and PDS-induced replication fork slowing in 411BR cells (Figure 5E). On the contrary, PARP inhibition prevented CPT- and PDS-induced replication fork slowing in hTERT-immortalized control human fibroblasts 1BR (Figure 5E). These data suggest that the DNA-ligase activity of the LIG4/XRCC4 complex is required for its role in promoting replication restart upon R-loop-mediated TRCs.

By EdU pulse labeling, we also tested whether the LIG4/XRCC4 complex was required for MiDAS in U2OS cells exposed to low dose of APH. We found that depletion of LIG4 or XRCC4 reduced the frequency of APH-induced EdU foci on metaphase chromosome spreads to levels comparable with those measured upon depletion of MUS81, RAD52 and POLD3, respectively (Figure 5F). Similar results were obtained with MRC5 fibroblasts (Figure S5B). In contrast, depletion of LIG3 or KU70 had no effect on MiDAS in APH-treated U2OS cells (Figure 5F). Consistent with the role of the LIG4/XRCC4 complex in MiDAS, depletion of LIG4 or XRCC4 decreased the number of concomitant DAPI-negative gaps on metaphase chromosomes and increased formation of 53BP1 nuclear bodies in G1 cells (Figure 5G, 5H and S5C).

Collectively, these results reveal a novel role for the LIG4/XRCC4 heterodimer in MUS81-mediated restart of replication forks stalled by R-loops.

Restart of replications forks stalled by R-loops requires active transcription

If R-loop-forming transcription complexes persisted ahead of restarting replication forks, they would again hinder replication fork progression, preventing TRC resolution. We therefore considered the possibility that after fork cleavage by MUS81/EME1, transcription is restarted and replication fork is reassembled after RNA polymerase passage through the lagging arm. In such scenario, replication restart at sites of TRCs would be impaired by inhibition of transcription elongation. To test this possibility, we first evaluated the effect of the transcription elongation inhibitors cordycepin and DRB on MiDAS in U2OS cells exposed to low dose of APH. Cordycepin and DRB were added together with EdU after release of cells from G2/M arrest to be present only during replication restart (Figure 6A and 6B). We found that both inhibitors significantly reduced the number of EdU foci and the concomitant DAPI-negative chromatid gaps on metaphase chromosome spreads (Figure 6A and S6A). In consistence with defective MiDAS, the frequency of anaphase bridges and micronuclei increased under these conditions (Figure 6C-6E). In addition, MiDAS was suppressed upon overexpression of RNaseH1 (Figure S6B), confirming that it is caused by R-loops.

In a second set of experiments, we measured the effect of cordycepin and DRB on the replication fork velocity in cells recovering from treatment with CPT or PDS. Again, the transcription inhibitors were added after removal of the R-loop inducing drugs. We found that both cordycepin and DRB inhibited replication fork progression after CPT or PDS removal (Figure 6F), suggesting that active transcription is also required for replication restart upon R-loop-mediated TRCs in S-phase. By monitoring KAP1 S824 phosphorylation, we also evaluated the effect of transcription inhibition on the level of chromosome breakage during the recovery from exposure of cells to CPT. As expected, we observed that treatment of U2OS cells with CPT following PARP inhibition dramatically increased the level of KAP1 S824 phosphorylation (Figure 6G, S6C and S6D). KAP1 S824 phosphorylation largely disappeared within 2 h after CPT removal, consistent with replication restart (Figure 6G and S6D). However, if DRB or cordycepin were present during the recovery, high levels of KAP1 S824 phosphorylation persisted as long as 6 h after CPT removal (Figure 6G and S6D). These findings suggest that fork religation and restart occur after the passage of the transcription complex.

DISCUSSION

Collisions between transcription and replication complexes represent a major intrinsic source of genomic instability in mammalian cells [77, 95]. Recent studies have revealed that impairment of replication fork progression by head-on transcription complexes is caused by the formation of co-transcriptional R-loops [75, 83]. In our study, we provide evidence that R-loop-provoked replication fork stalling is an active process that involves RAD51-mediated fork reversal. This restrains resumption of DNA replication through a process involving cleavage of the leading arm of the stalled fork by MUS81/EME1 endonuclease followed by fork religation mediated by the LIG4/XRCC4 complex after reannealing of the parental DNA strands by RAD52 (Figure 7). The switch from the active fork stalling to replication restart is mediated by the RecQ DNA helicases RECQ1 and RECQ5. RECQ1 converts reversed forks to the original three-way structure, while RECQ5 disrupts RAD51 nucleoprotein filaments assembled on stalled forks prior to a new round of fork reversal, thereby generating suitable substrate for MUS81/EME1 endonuclease (Figure 7). Consistently, RECQ5 depletion causes replication fork stalling in actively transcribed genes and accumulation of RAD51 nuclear foci formed as a consequence of transcription-replication interference [129]. We propose that replication fork cleavage by MUS81/EME1 is required to relieve the positive DNA supercoiling generated between converging transcription and replication machineries (Figure 7), which halts their progression and probably triggers R-loop formation [75, 95]. This would allow reactivation of RNA synthesis upon R-loop unwinding and passage of the transcription complex across the replication-stalling site, eliminating the obstacle to replication fork progression (Figure 7). Along this line, we found that restart of replication forks stalled by R-loops was impaired by transcription elongation inhibitors, leading to persistence of DNA breaks (Figure 6). Thus, the controlled fork cleavage/religation cycle would ensure the movement of the replication machinery through oppositely transcribed DNA regions without disruption of transcription complexes. This would be particularly relevant for the longest human genes where TRCs occur during each transcription cycle because it takes longer than one cell cycle [114].

We show that MiDAS, the prophase-specific DNA-repair synthesis induced by mild replication stress at CFSs [166], depends on R-loop formation and requires the same set of factors as restart of R-loop-stalled replication forks in S-phase. However, the notable difference between the processing of stalled replication forks in S-phase and in early mitosis is that the binding of MUS81 to SLX4, which is essential for MUS81/EME1 recruitment to replication stalling sites [166] (Figure 3I), is enhanced upon entry to mitosis through CDK1-

mediated phosphorylation of the SLX4's SAP domain that binds to MUS81 [195, 196]. As a result, MUS81 is markedly enriched on CFSs in mitotic prophase [166, 191]. We propose that this phosphorylation-driven enhancement of MUS81/SLX4 complex formation serves to ensure that all persistent replication intermediates are resolved before the onset of anaphase.

Previous studies have postulated that MUS81-initiated restart of DNA synthesis at stalled replication forks occurs by BIR, which is a conservative form of DNA replication [161, 166, 183, 184]. We show here that the nascent DNA strands generated during MiDAS segregate, in case of the majority of MiDAS events, with both sister chromatids, which is indicative of a semiconservative mode DNA replication. Moreover, we demonstrate that the nascent DNA strands synthesized after replication restart at R-loops in S-phase are sensitive to HU-induced resection in BRCA2-deficient cells. As this process is initiated from reversed forks [157], our data suggest that the MUS81 pathway initiates semiconservative DNA replication, at least upon replication fork stalling by R-loops. Studies in yeast have shown that BIR-mediated restart of collapsed replication forks is largely dependent upon the Rad51 recombinase, which mediates BIR initiation by catalyzing D-loop formation [198]. However, the human RAD51 and its loader BRCA2 are not required for MiDAS and restart of R-loop-stalled replication forks in S-phase [156, 165] (Figure 2D). Instead, RAD51 restrains replication restart by promoting fork reversal [156]. It should be noted that the evidence for the involvement of POLD3 and RAD52 in BIR has been provided by experiments using a reporter assay for BIR-mediated repair of a two-ended DSB, which is dependent on RAD51 and BRCA2 [161]. Thus, we conclude that RAD51-dependent BIR does not play a major role in restart of DNA synthesis upon R-loop-mediated TRCs.

In a fraction of MUS81-dependent MiDAS events, nascent DNA appeared to segregate only with one sister chromatid (Figure 4C and S4B-D). These events were attributed to a RAD51-independent BIR-like process that occurs through annealing of short homologous sequences [165]. It should be noted that BIR initiated at sites of microhomology is mutagenic as it can generate copy-number variations and complex chromosomal changes [203, 204]. In contrast, the mechanism for replication restart revealed by our study allows accurate completion of genome duplication, which is desirable for mammals to avoid malignant transformations. Future studies are needed to clarify the molecular mechanisms underlying the usage of these two replication restart pathways in the cellular response to R-loop-mediated replication stress.

ACKNOWLEDGEMENTS

We thank Agata Smogorzewska and Patrick Calsou for cell lines, Stefano Ferrari for comments on the manuscript, and Christiane König and Sebastian Ursich for technical assistance. This work was supported by grants from the Swiss National Science Foundation (31003A_166451), Novartis Foundation for Medical-biological Research, Swiss Cancer League (KFS-3802-02-2016), Czech Science Foundation (17-02080S) and Stiftung zur Krebsbekämpfung. J.D. was supported by the Neuron Fund for Support of Science. M.L. and R.Z. were supported by the Swiss National Science Foundation Grant 31003A_169959 and the ERC Consolidator Grant "ReStreCa" (617102).

STAR METHODS

CONTACT FOR REAGENT AND RESOURCE SHARING

Further information and requests for reagents may be directed to, and will be fulfilled by, the lead contact, Dr. Pavel Janscak (pjanscak@imcr.uzh.ch).

EXPERIMENTAL MODEL AND SUBJECT DETAILS

Source of cell lines used in the study is reported in the Key Resources Table.

METHOD DETAILS

Plasmid construction

The M27 variant of human RNase H1, lacking first 26 amino acids that contain mitochondrial targeting signal, was used in this study. The EcoRI-NotI fragment of a pEGFP-N2 derivative containing hM27 RNase H1 ORF C-terminally fused to enhanced green fluorescence protein (EGFP) (kindly provided by Dr. Kanagaraj Radhakrishnan) was blunted by large Klenow fragment and subcloned into the EcoRV site of the plasmid pAIO [129]. A DNA oligoduplex encoding for an shRNA to silence endogenous RNase H1 (target region: nucleotides 730-751) was introduced between BglII and HindIII sites of the pAIO vector. Top strand: (5'GATCTACGATAAATGGTATAACTAACCTCGAGGTTAGTTATACCATTTATCGTT TTTTCTGCAGA-3');

Bottom strand: (5'-AGCTTCTGCAGAAAAAACGATAATGGTATAACTAAC CTCGAGGTTAGTTATACCATTTATCGTA-3'). The NotI-HindIII fragment of the pAIO [shRNH1] construct containing the shRNA expression cassette was ligated with the HindIII-NotI fragment of the pAIO [RNH1-EGFP] construct containing the hM27 RNaseH1-EGFP

gene. In the resulting plasmid, seven silent mutations were introduced in to the RNase H1 cDNA between the nucleotides 730-751 to render the resulting RNase H1 transcript resistant to the shRNA. The following primers were used for two-round mutagenesis (underlined nucleotides were mutated):

RNase H1_MTG730_1F:

5'-CAGACAGTATGTTTACCATCAACGGCATAACTAACTGGGTTCAAGG-3'

RNase H1_MTG730_1R:

5'-CCTTGAACCCAGTTAGTTATGCCGTTGATGGTAAACATACTGTCTG-3'

RNase H1_MTG730_2F:

5'-GTTTACCATCAACGGCATCACGAATTGGGTTCAAGGTTGG-3'

RNase H1_MTG730_2R:

5'-CCAACCTTGAACCCAATTCGTGATGCCGTTGATGGTAAAC-3'

Cell culture

U2OS, HeLa, MRC5 and VA13 cells were grown in Dulbecco's Modified Eagle Medium (DMEM; Thermo Fisher Scientific), supplemented with 10% fetal calf serum (FCS; Thermo Fisher Scientific) and streptomycin/penicillin (100 U/ml), at 37°C in a humidified incubator containing 5% CO_2. Clones of U2OS T-REx cells stably transfected with the pAIO [RNH1-EGFP/shRNH1] construct (U2OS T-REx/RNH1-GFP) were selected in the presence of 1 μg/ml puromycin (InvivoGen). Positive clones were identified by testing for expression of GFP-tagged RNase H1 by western blotting using anti-GFP antibody, before and after doxycycline (1 ng/ml) induction for 24 h. U2OS T-REx stable cell lines carrying pAIO-based vectors for expression of Flag-tagged versions of wild-type RECQ5, RECQ5F666A and RECQ5K58R were described previously [129]. To induce expression of RECQ5 variants, doxycycline was added to a concentration of 0.4-1.0 ng/ml. Expression level of exogenous RECQ5 was tuned to be comparable with the level of endogenous RECQ5 by adjusting doxycycline concentration. U2OS T-REx cell lines were cultivated in DMEM supplemented with 10% FBS (Tet-free approved), streptomycin/penicillin (100 U/ml), 50 μg/ml hygromycin B and 1 μg/ml puromycin. Human FA complementation group P (FA-P; SLX4 deficiency) fibroblast cell line, RA3331, transformed using HPV6 and E7 proteins and immortalized with a human catalytic subunit of telomerase hTERT (RA3331/E6E7/hTERT), and its derivatives expressing HA-tagged wild type SLX4 or SLX4 ΔSAP were grown in DMEM supplemented with 15% FBS, 2 μg/ml puromycin and streptomycin/penicilllin (100 U/ml) [194]. Human telomerase reverse transcriptase-immortalized human fibroblasts 1BR

(control) and 411BR (isolated from a LIG4 syndrome patient) were grown in DMEM supplemented with 15% FBS and streptomycin/penicillin (100 U/ml) [202].

Small-interfering RNA transfections

Transfections of siRNAs (a final concentration of 40 nM) were done at 30-40% confluency using Lipofectamine RNAiMAX (Invitrogen) according to the manufacturer's instructions. 24 h after siRNA transfection, the medium was exchanged with fresh medium. The sequences of the sense strand of siRNA duplexes are listed in the Key Resources Table. For ectopic expression of RECQ5 variants in stable U2OS T-REx cell lines, endogenous RECQ5 was depleted by transfection of RECQ5 siRNA_2 for a total time of 72 h. Twenty-four hours after siRNA transfection, doxycycline (0.4-1.0 ng/ml) was added to induce expression of RECQ5 variants for a further 48 h. Where siRECQ5, siRAD52 and siLIG4 are indicated, cells were transfected with RECQ5 siRNA_1, RAD52 siRNA_1 and LIG4 siRNA_1, respectively. For experiment in Figure 5D, RAD52 siRNA_2 was used.

Preparation cell extracts and western blot analysis

Cells were suspended in lysis buffer [50 mM Tris-HCl buffer (pH 7.5), 120 mM NaCl, 20 mM NaF, 1 mM EDTA, 6 mM EGTA, 15 mM Na-Pyrophosphate and 0.5% (v/v) NP-40] supplemented with 1 mM benzamidine, 0.2 mM PMSF, 0.5 mM sodium orthovanadate and protease inhibitor cocktail (Complete, EDTA-free; Sigma-Aldrich), and sonicated for 7 min with a Diagenode sonicator. Cellular debris was isolated from soluble fraction by centrifugation at 12,000 rpm for 30 min at 4°C and protein concentration was measured by Bradford assay. 30-60 µg of total protein from cell lysates were loaded onto 8%-10% SDS-PAGE gels. After electrophoresis, separated proteins were transferred from gel onto a nitrocellulose membrane in a wet-transfer apparatus (Bio-rad) with buffer containing 10% ethanol and 90% 1x transfer buffer (transfer buffer 10x: 25 mM tris, 192 mM glycine, 10% methanol) at 100 V for 2 h in cold room at 4°C. The membrane was blocked with 2% ECL blocking solution in TBS-T [20 mM Tris-HCl (pH 7.4), 150 mM NaCl, 0.1% (v/v) Tween-20] for 30 min. Afterwards, the membranes were incubated with the primary antibodies in 4% ECL blocking solution at 4°C O/N. The membranes were then washed 3 times in TBS-T and incubated with appropriate horseradish peroxidase-coupled (HRP) secondary antibody in 2% ECL blocking solution for 60 min at RT. Afterwards, the membranes were washed three times with TBS-T and protein bands were detected by luminol-based reaction using a chemiluminescence reagent (Pierce). The primary antibodies used for western blotting:

FLAG mouse monoclonal (F1804, Sigma-Aldrich; 1:500 dilution), BRCA1 (D-9) mouse monoclonal (sc-6954, Santa Cruz Biotechnology; 1:1000 dilution), MUS81 (Clone MTA30 2G10/3) mouse monoclonal (M1445, Sigma-Aldrich; 1:1000 dilution), Ku p70 (Ab-4) mouse monoclonal (MS329-P1, Thermo Fisher Scientific; 1:1000 dilution), SLX4 rabbit polyclonal (A302-270A, Bethyl Laboratories; 1:1000 dilution), TFIIH p89 (S-19) rabbit polyclonal (sc-293, Santa Cruz Biotechnology; 1:1000 dilution), GFP rabbit polyclonal (ab290, Abcam; 1:1000 dilution), RAD51 rabbit polyclonal (sc-8349; Santa Cruz Biotechnology; 1:1000 dilution), RECQ5 rabbit polyclonal (Janscak lab; 1:1000 dilution), RECQ1 rabbit polyclonal (NB100-182, Novus Biological; 1:1000 dilution), KAP1 pS824 rabbit polyclonal (ab70369, Abcam; 1:1000 dilution), KAP1 rabbit polyclonal (A300-274A, Bethyl Laboratories; 1:1000 dilution), LIG4 (D-8) mouse monoclonal (sc-271299, Santa Cruz Biotechnology; 1:500 dilution), XRCC4 (C-4) mouse monoclonal (sc-271087, Santa Cruz Biotechnology; 1:500 dilution), LIG3 (E-7) mouse monoclonal (sc-390992, Santa Cruz Biotechnology; 1:500 dilution), BRCA2 (Ab-1) mouse monoclonal (OP-95, EMD Millipore; 1:000 dilution), RAD52 (H300) rabbit polyclonal (sc-8350, Santa Cruz Biotechnology; 1:500 dilution), POLD3 (M01, clone 3E2) mouse monoclonal (H00010714-M01, Abnova; 1:1000 dilution), ZRANB3 rabbit polyclonal (23111-1-AP, Proteintech; 1:1000 dilution), EME1 (MTA31 7h2/1) mouse monoclonal (sc-53275, Santa Cruz Biotechnology; 1:1000 dilution). Secondary antibodies used for western blotting: goat anti-rabbit IgG-HRP (A5050, Sigma-Aldrich; 1:1000 dilution), goat anti-mouse IgG HRP (A4416, Sigma-Aldrich; 1:2000 dilution).

Immunofluorescence assays

Cells grown on autoclaved coverslips were transfected with siRNA and/or treated with drugs. After the treatment, cells were washed two times with 1x PBS and pre-extracted for 15 min with ice cold 1x PBS containing 0.5% (v/v) Triton X-100. Then the cell were washed three times with 1xPBS and fixed with 4% formaldehyde for 10 min at RT. For KAP1-pS824 immunofluorescence, cells were fixed with 4% formaldehyde for 10 min at RT without pre-extraction. After three washes with 1x PBS, fixed cells were permeabilized in 1x PBS containing 0.2% (v/v) Triton X-100 for 10 min at RT. Cells were then washed with PBS and blocked in 5% BSA/1x PBS solution for 45 min. Cover slips were then incubated O/N at 4°C with appropriate primary antibodies diluted in 5% BSA/1x PBS. The following day, cover slips were washed three times with 1x PBS and incubated for 60 min at RT with secondary antibodies diluted in 5% BSA/1x PBS. After three washes with 1x PBS, cover slips were incubated with 1 μg/ml DAPI/1x PBS for 15 min in dark at RT. Then the coverslips were

washed twice with 1x PBS and mounted with Vectashield antifade medium. The mounted slides were left to dry at RT for 30 min and then sealed with nail polish. Images were acquired with a Leica DM6B upright fluorescent microscope (63x/1.40 Oil immersion) and analyzed with the tools of ImageJ. The DAPI signal was used for generation of an intensity threshold-based mask to identify individual nuclei. This mask was applied to measure nuclear foci number or mean nuclear fluorescence intensity in different channel for each nucleus by using speckle inspector tool in BioVoxxel Toolbox plugin and mean intensity measurement tool, respectively. The primary antibodies used for the immunofluorescence staining: MUS81 (MTA30 2G103) mouse monoclonal (sc-53382, Santa Cruz Biotechnology; 1:500 dilution), 53BP1 rabbit polyclonal (sc-22760, Santa Cruz Biotechnology; 1:500 dilution), Cyclin A (B-8) mouse monoclonal (sc-271682, Santa Cruz Biotechnology; 1:50 dilution), KAP1 pS824 rabbit polyclonal (ab70369, Abcam; 1:250 dilution), FANCD2 rabbit polyclonal (NB100-182, Novus Biologicals; 1:500 dilution). Secondary antibodies used for immunofluorescence staining: Alexa Fluor 488 Goat Anti-Rabbit IgG (A110334, Thermo Fisher Scientific; 1:300 dilution), Alexa Fluor 594 Goat Anti-Rabbit IgG (A11037, Thermo Fisher Scientific; 1:300 dilution), Alexa Fluor 488 Goat Anti-Mouse IgG (A11001, Thermo Fisher Scientific; 1:300 dilution), Alexa Fluor 594 Goat Anti-Mouse IgG (A11005, Thermo Fisher Scientific; 1:300 dilution),.

Analysis of anaphase chromatin bridges and micronuclei

For analysis of anaphase chromatin bridges, cells grown on cover slips were treated with 0.4 μM aphidicolin and 9 μM RO-3306 for 16 h. Then the cells were washed three times with 1x PBS for 5 min at RT and released in the fresh medium for 80 min at 37°C. In case of micronuclei analysis, cells, after treatment with 9 μM RO-3306 and 0.4 μM aphidicolin for 16 hours, were washed three times with 1x PBS and released in the fresh medium for 30 min. Prometaphase cells were then shaken off, pelleted and re-seeded onto poly-lysine coated glass coverslips in medium containing 3 μM cytochalasin B, and allowed to progress in to the subsequent G1 phase (145 min) at 37°C in a humid atmosphere with 5% CO2. After the respective treatment, cells were washed twice with 1x PBS and fixed with 4% formaldehyde for 10 min at RT. After fixation, cells were washed three times with 1xPBS and permeabilized using ice-cold 0.2% (v/v) Triton X-100 in 1x PBS for 10 min at RT. Then the cells were washed three times with 1x PBS and stained with DAPI. Images were acquired with a Leica DM6B upright fluorescent microscope (63x/1.40 Oil immersion).

Quantifications of the frequencies of chromatin bridges in anaphase cells and micronuclei in G1 daughter cells were done manually with the help of ImageJ.

Analysis of metaphase chromosome spreads and MiDAS assay

Cells seeded in 10-cm dishes were treated with 9 μM RO-3306 in combination with 0.4 μM aphidicolin for 16 hours. Cells were subsequently washed three times with 1x PBS for 5 min and then released in fresh medium (pre-warmed to 37°C) containing 0.1 μg/ml Colcemid for 60 min. In the case of MiDAS analysis, cells were released to medium containing 20 μM 5-ethynyl-2′-deoxyuridine (EdU) and 0.1 μg/ml Colcemid for 60 min. Metaphase cells were collected by shake-off and centrifugation at 1200 rpm for 5 min. After one wash with 1x PBS, cells were swollen by incubation in 75 mM KCl (pre-warmed to 37°C) for 20 min at 37°C. Swollen mitotic cells were collected at 1200 rpm for 5 min, fixed using methanol:acetic acid (3:1), and dropped onto pre-hydrated glass slides and aged for up to 24 h. Chromosome spreads were mounted with Vectashield mounting medium containing DAPI. Images were acquired using a Leica DM6B upright fluorescent microscope at (63x/1.40 Oil immersion). For MiDAS analysis, metaphase spread slides were aged for 24 h followed by EdU detection using Click-IT Plus EdU Alexa fluor 488 Imaging Kit (Thermo Fisher Scientific) and chromosomes stained with Vectashield mounting medium containing DAPI. Images were captured using a Leica SP8 upright confocal laser-scanning microscope (63x/1.40 Oil immersion). Quantifications of DAPI-negative gaps and EdU incorporation events (twin foci and complex foci were counted as one event) on metaphase chromosome spreads was done manually with help of ImageJ.

DNA fiber spreading assay

Cells were labeled with 30 μM 5-chloro-2'-deoxyuridine (CldU) for 30 min, washed three times with 1x PBS, and then labeled with 250 μM 5-iodo-2'-deoxyuridine (IdU) for 30 min. After labeling, cells were washed three times with 1x PBS, quickly trypsinized and re-suspended in 1x PBS to a concentration of 250,000 cells per ml. The labeled cells were diluted 1:3 with unlabeled cells, and 2.5 μl of this cell suspension were mixed with 7.5 μl of lysis buffer [200 mM Tris-HCl (pH 7.5), 50 mM EDTA, 0.5% (w/v) SDS] on a glass slide by gently stirring with a pipette tip. After 9-min incubation at RT, the slides were tilted at 30°-40°, the surface tension of the drops was disrupted by a tip and the drops were allowed to run down the slides slowly. The DNA spreads were air-dried and fixed in methanol/acetic acid (3:1) at 4°C overnight. DNA fibers were denatured with 2.5 M HCl for 1 h at RT, washed

four times with 1x PBS and blocked with 2% BSA in 1x PBS for 40 min. After blocking, slides were incubated for 2.5 h in the dark at RT with rat monoclonal anti-BrdU antibody (ab6326, Abcam; 1:500 dilution) to detect CldU and mouse monoclonal anti-BrdU antibody (347580, BD Biosciences; 1:100 dilution) to detect IdU. Slides were then washed four times with 1x PBST (PBS supplemented with 0.2% Tween-20) and incubated with secondary antibodies, donkey anti-rat Cy3 (712-166-153, Jackson ImmunoResearch; 1:150 dilution) and goat anti-mouse Alexa 488 (A110334, Thermo Fisher Scientific; 1:300 dilution), for 2 h in the dark at RT. After washing four times with 1x PBST, the slides were air-dried in the dark for 40 min at RT and mounted with ProLong Gold antifade mounting medium (25µl per coverslip 24x50 mm). Images were acquired with a Leica DM6B upright fluorescent microscope (63x/1.40 Oil immersion). CldU and IdU tract lengths (µm) were measured by using segmented line tool of ImageJ.

Electron microscopy

Electron microscopy analysis was performed as described [156], with minor modifications. Briefly, cells were collected, washed one time with and re-suspended in 1x PBS. *In vivo* psoralene cross-linking of the DNA was achieved by repetitive (twice) cross-linking with 4,5′, 8-trimethylpsoralen (10 µg /ml final concentration) in dark for 5 min, followed by irradiation pulses with UV 365 nm monochromatic light (UV Stratalinker 1800) for 3 min. For DNA extraction, cells were lysed in lysis buffer [40 mM Tris-HCl (pH 7.5), 1.28 M sucrose, 20 mM $MgCl_2$, and 4% (v/v) Triton X-100] and digested with digestion buffer [800 mM guanidine-HCl, 30 mM Tris-HCl (pH 8.0), 30 mM EDTA (pH 8.0), 5% (v/v) Tween-20, and 0.5% (v/v) Triton X-100] at 50 °C for 2 h in presence of 1 mg/ml proteinase K. The DNA was purified by phase separation method using chloroform/isoamylalcohol (24:1) with centrifugation at 8000 rpm for 20 min using a Sorvall LYNX 600 centrifuge. DNA was precipitated by adding equal volume of isopropanol to the upper phase collected in the previous step. Finally, the DNA was washed with 70% Ethanol and disolved in 200 µl TE (Tris-EDTA) buffer. 100 U of the restriction enzyme PvuII were used to digest 12 µg of the isolated genomic DNA in 250 µl of 1x CutSmart buffer (New England Biolabs) for 5 h, and to eliminate RNA contamination, 6 µl of 10 mg/ml RNase A was added during the last 3 h. Replication intermediates enrichment was performed by QIAGEN Plasmid Mini Kit (100) columns. The surface tension of QIAGEN-tip 20 columns was reduced by applying 1 ml QBT buffer. The columns were then washed with 10 mM Tris-HCl (pH 8.0), 1 M NaCl and equilibrated with 10 mM Tris-HCl (pH 8.0), 300 mM NaCl. After loading of DNA, columns

were washed with 10 mM Tris-HCl (pH 8.0) containing 900 mM NaCl. DNA was eluted with caffeine solution [10 mM Tris-HCl (pH 8.0), 1 M NaCl and 1.8% (w/v) caffeine]. To purify and concentrate the DNA, an Amicon size-exclusion column was used. DNA was then resuspended in TE buffer. The benzyldimethylalkylammonium chloride (BAC) method was used to spread the DNA on water surface and then to load it on carbon-coated 400-mesh copper grids. Subsequently, DNA was coated with platinum using a high vacuum evaporator MED 020 (BalTec). Microscopy was performed with a transmission electron microscope (Tecnai G2 Spirit; FEI; LaB6 filament; high tension ≤120 kV) equipped with a side mount charge-coupled device camera (2600 × 4000 pixels; Orius 1000; Gatan, Inc.). Images were processed and analyzed with DigitalMicrograph version 1.83.842 (Gatan, Inc.) and ImageJ (National Institutes of Health), respectively.

Pulsed-field gel electrophoresis

Cells were harvested by trypsinization and washed once with 1x PBS. Then the cells were resuspended in 1x PBS (1.0×10^6 cells/50 µl). Agarose plugs of 1.0×10^6 cells were prepared in a disposable plug mold (Bio-Rad Laboratories) by mixing (1:1) of 2% (w/v) SeaPlaque GTG agarose in 1xPBS and cell suspended in 1xPBS. Plugs were incubated in lysis buffer [100 mM EDTA, 1% (w/v) sodium lauroyl sarcosinate, 0.2% (w/v) sodium deoxycholate, and 0.5 mg/ml proteinase K] at 37 °C for 72 h and then washed four times in 20 mM Tris-HCl (pH 8.0) buffer containing 50 mM EDTA for 5 min each time on shaker before loading onto 0.9% (w/v) Pulsed Field Certified agarose (Bio-Rad) prepared in Tris-borate/EDTA buffer. Electrophoresis was performed in a pulsed-field gel electrophoresis apparatus, CHEF DR III varible angle system (Bio-Rad), run in Tris-borate/EDTA buffer for 21 h at 14 °C according to the following protocol (block I: 9 h, 120° included angle, 5.5 V cm^{-1}, 30–18 s switch; block II: 6 h, 117° included angle, 4.5 V cm^{-1}, 18–9-s switch; block III: 6 h, 112° included angle, 4.0 V cm^{-1}, 9–5 s switch). Gels were stained with ethidium bromide and gel images were acquired by an AlphaImager™ system (Alpha Innotech Corporation). DNA bands were quantified using ImageJ. For each lane, the mean intensity of the band corresponding to broken DNA was divided by the mean intensity of the band corresponding to intact DNA. The resulting values were normalized to the value obtained for control condition (taken as 100%).

QUANTIFICATION AND STATISTICAL ANALYSIS

Statistical analysis was performed with GraphPad Prism 7 (GraphPad Software) using unpaired t-test or Mann-Whitney test, where appropriate.

SUPPLEMENTAL TABLES

Table S1, related to Figures 1 and 2. Electron microscopy data for experiments in Figures 1F, 2F and S2E. (A-B) Percentage of observed reversed forks (% RF) in two independent experiments (Exp_1 and Exp_2) for samples in Figure 1F (A), 2F (B) and S2E (C). Numbers of analyzed DNA molecules in brackets.

A

U2OS T-REx	NT	PDS			CPT		
	DMSO	DMSO	+CORD	+RNase H1	DMSO	+CORD	+RNase H1
% RF Exp_1	5 (99)	15 (94)	6 (99)	7 (90)	27 (94)	10 (94)	12 (94)
% RF Exp_2	7 (72)	18 (71)	11 (71)	10 (74)	28 (67)	12 (72)	14 (74)

B

U2OS	siLUC		siMUS81		siSLX4		siRECQ5		siMUS81+ siRECQ5		siMUS81+ siSLX4	
CPT	-	+	-	+	-	+	-	+	-	+	-	+
% RF Exp_1	5 (70)	27 (81)	16 (84)	39 (82)	20 (77)	37 (93)	20 (74)	39 (77)	21 (71)	38 (87)	20 (62)	38 (81)
% RF Exp_2	6 (71)	26 (80)	17 (74)	38 (75)	16 (80)	36 (77)	16 (70)	42 (70)	18 (80)	35 (75)	17 (74)	36 (79)

C

U2OS T-REx	WT			F666A			K58R		
siRECQ5	-	+	+	-	+	+	-	+	+
Dox	-	-	+	-	-	+	-	-	+
% RF Exp_1	7 (100)	16 (100)	9 (100)	8 (100)	17 (101)	18 (100)	8 (100)	16 (101)	17 (97)
% RF Exp_2	8 (71)	20 (60)	10 (71)	8 (71)	18 (60)	18 (70)	9 (70)	17 (71)	19 (67)

Chappidi et al., Figure 1

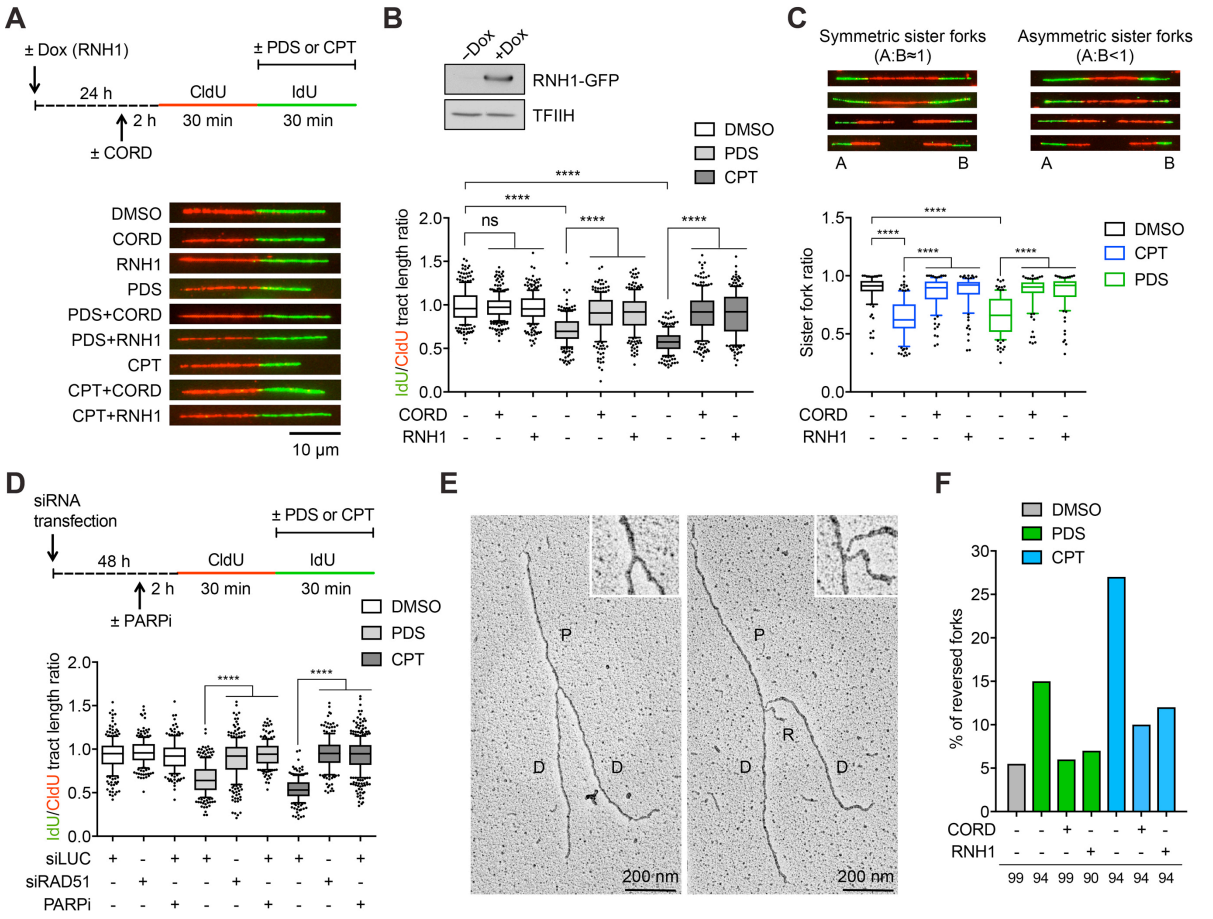

Figure 1. Factors responsible for replication fork slowing induced by pyridostatin or camptothecin.

(A) Effect of RNase H1 (RNH1) overexpression and transcription inhibition on replication fork slowing induced by pyridostatin (PDS; 10 µM) or camptothecin (CPT, 100 nM) in U2OS T-REx/RNH1-GFP cells. *Top panel*: Experimental workflow of DNA fiber assays. Expression of RNH1-GFP transgene was induced by addition of doxycycline (+Dox; 1 ng/ml). Transcription was inhibited by addition of 50 µM cordycepin (CORD) 2 h prior to replication tract labeling with CldU and IdU. Cells were mock-treated (DMSO) or treated with CPT/PDS during IdU labeling. *Bottom panel*: Representative images of replication tracts detected on DNA fibers of cells treated as indicated. (B) Box plot of values of IdU/CldU tract length ratio for conditions in (A) obtained in three independent experiments (n ≥ 200, whiskers: 10-90 percentiles). ns, not significant; ****P < 0.0001 (Mann-Whitney test). (*Top panel*) A western blot showing expression of RNH1-GFP upon induction with Dox for 24 h. (C) PDS and CPT induce sister fork asymmetry in a manner dependent on the formation of co-transcriptional R-loops. *Top panel*: Representative images of symmetric and asymmetric replication tracts of sister forks identified on DNA fibers in (A). *Bottom panel*: Box plot of values of sister fork IdU tract length ratio measured for indicated conditions (n ≥ 100, whiskers: 10-90 percentiles)..****P < 0.0001 (Mann-Whitney test). (D) Effect of CPT (100 nM) and PDS (10 µM) on replication fork progression in U2OS cells upon PARP inhibition or RAD51 depletion. *Top panel*: Experimental workflow of DNA fiber assays. PARP activity was blocked by addition of the PARP inhibitor (PARPi) olaparib (10 µM) at 2 h prior to DNA fiber labeling. *Bottom panel*: Box plot of values of IdU/CldU tract length ratio obtained

for indicated conditions in three independent experiments (n ≥ 200, whiskers: 10-90 percentiles). ns, not significant; ****P < 0.0001 (Mann-Whitney test). (E) Representative electron micrographs of normal (left) and reversed (right) replication forks observed on genomic DNA of U2OS T-REx/RNH1-GFP cells after treatment with 100 nM CPT for 1h. P, parental duplex; D, daughter duplex; R, regressed arm. (F) Effect of transcription inhibition and RNH1 overexpression on the frequency of reversed replication forks in U2OS T-REx/RNH1-GFP cells treated with CPT (100 nM) or PDS (10 μM) for 1 h. Where indicated RNH1-GFP expression was induced by addition of Dox at 24 h prior to treatment. CORD (50 μM) was added 2 h prior to addition of CPT or PDS. The numbers in brackets indicate the number of analyzed molecules. Similar results were obtained in an independent experiment (Table S1A).

Chappidi et al., Figure 2

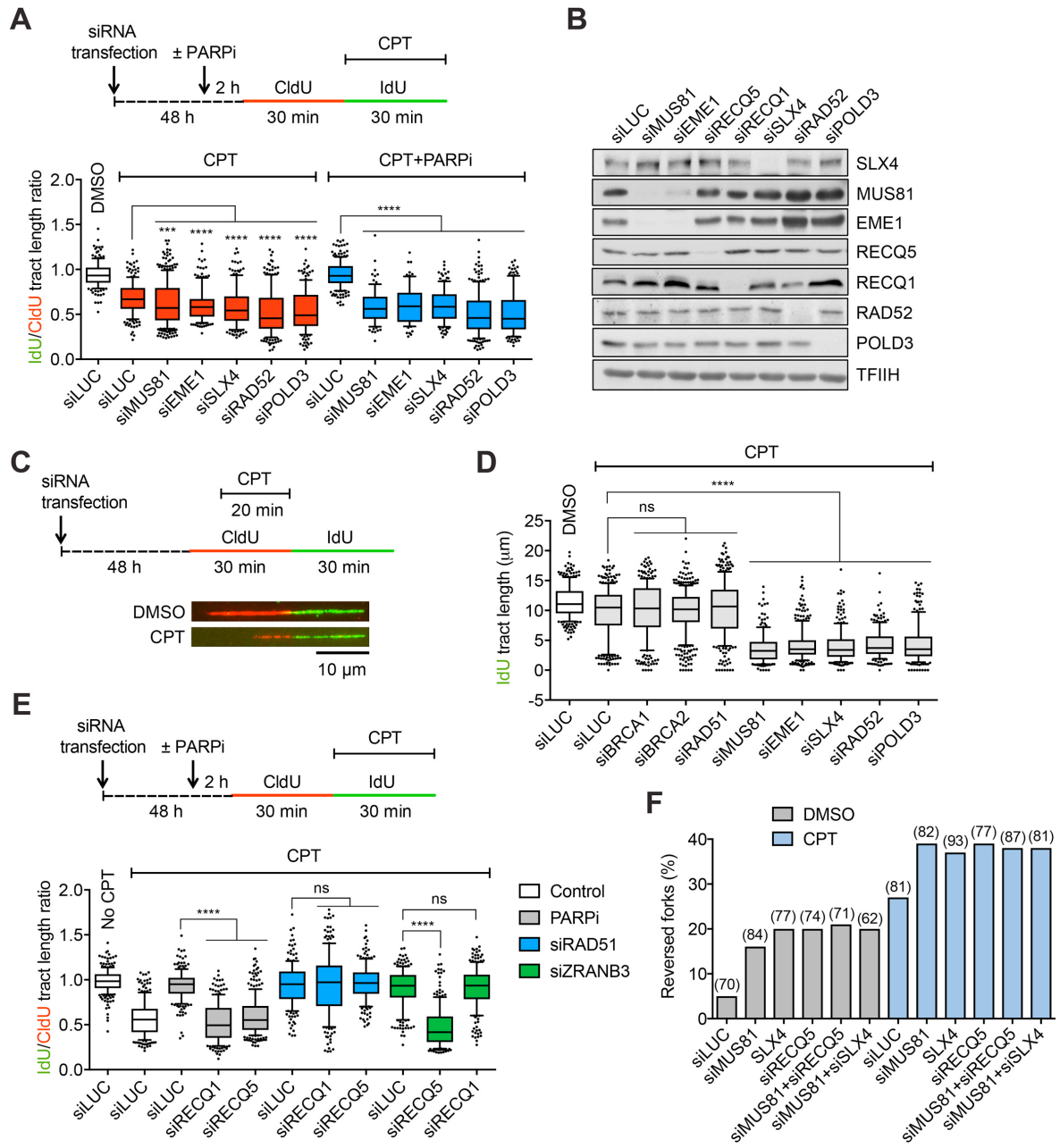

Figure 2. Factors required for replication restart upon R-loop-mediated TRCs
(A) Effect of depletion of MUS81, EME1, SLX4, RAD51 and POLD3, respectively, on the replication fork velocity in U2OS cells upon treatment with 100 nM CPT, and on the rescue of CPT-induced replication fork slowing by PARP inhibition with 10 µM olaparib (PARPi). *Top panel*: Experimental workflow of DNA fiber assays. *Bottom panel*: Box plot of values of IdU/CldU tract length ratio obtained for indicated conditions in three independent experiments ($n \geq 200$, whiskers: 10-90 percentiles). ns, not significant; ***P < 0.001, ****P < 0.0001 (Mann-Whitney test). (B) Western blot analysis of extracts of U2OS cells transfected with indicated siRNAs. Cells were harvested 48 h post siRNA transfection. (C) Experimental workflow of replication recovery assays and representative images of replication tracts detected on DNA fibers of mock-depleted (siLUC) U2OS cells. Cells were

labeled sequentially with IdU and CldU for 30 min each. Where indicated, CPT (100 nM) or DMSO (mock treatment) were added during the last 20 min of the CldU pulse. (D) Effect of depletion of the indicated proteins on replication fork velocity after treatment of U2OS cells with CPT. At least 200 IdU tracts were measured for each condition in three independent experiments. Whiskers indicate 10-90 percentiles. ns, not significant; ****P < 0.0001 (Mann-Whitney test). (E) Effects of depletion of RECQ1 or RECQ5 on the rescue of replication fork slowing in CPT-treated U2OS cells by PARP inhibition and RAD51 or ZRANB3 depletion, respectively. *Top panel*: Experimental workflow of DNA fiber assays. *Bottom panel*: Box plot of values of IdU/CldU tract length ratio obtained for indicated conditions in three independent experiments (n ≥ 200, whiskers: 10-90 percentiles). ns, not significant; ****P < 0.0001 (Mann-Whitney test). (F) Frequency of reversed replication forks in U2OS cells transfected with indicated siRNAs. Where indicated, cells were treated with 100 nM CPT. The numbers in brackets indicate the number of analyzed molecules. Similar results were obtained in an independent experiment (Table S1B). Also see Figure S1 and S2.

Chappidi et al., Figure 3

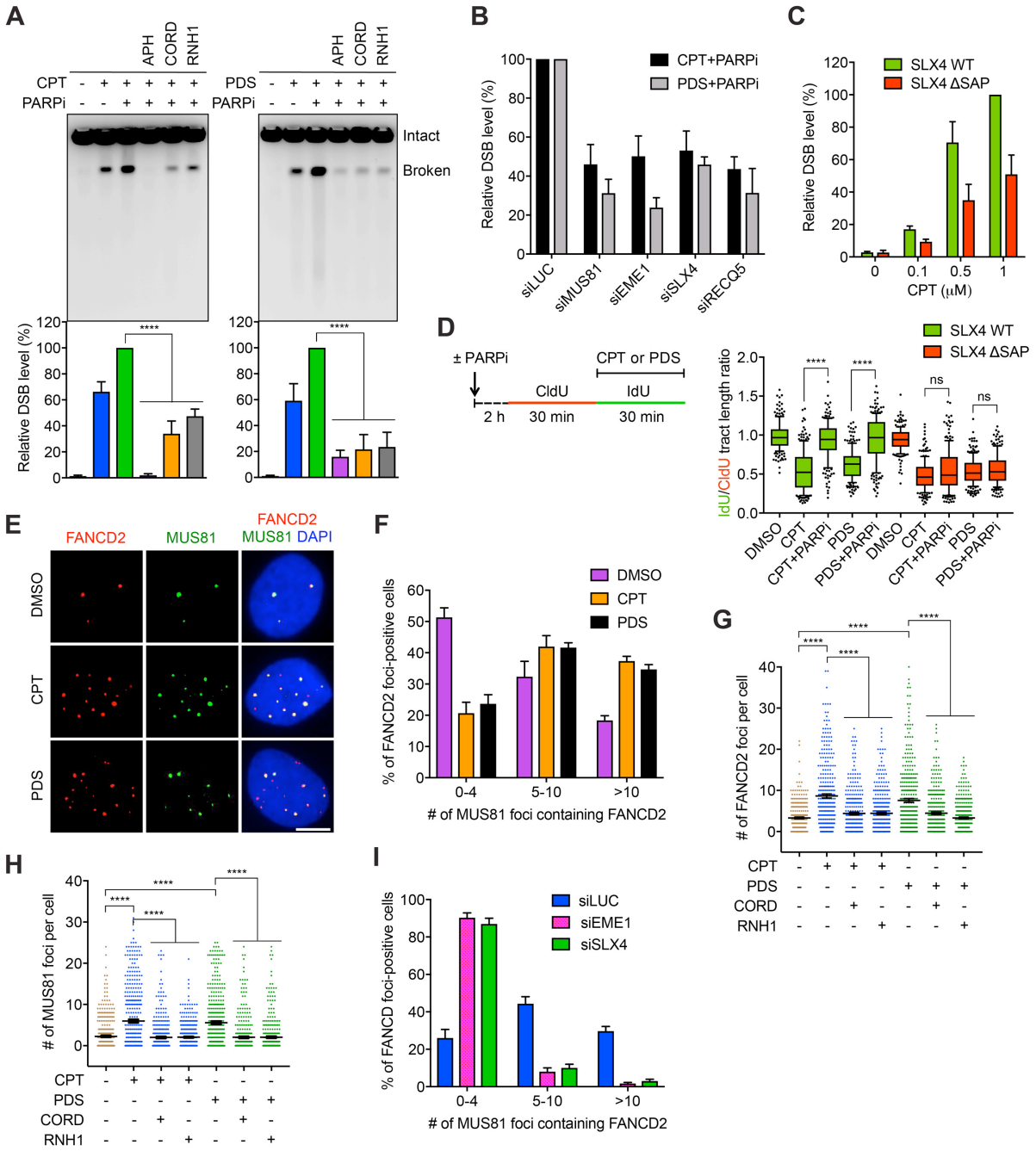

Figure 3. Replication restart upon R-loop-mediated TRCs depends on fork cleavage by MUS81 endonuclease.

(A) Genomic DNA breakage stimulated by PARP inhibition (PARPi) in CPT- and PDS-treated U2OS T-REx/RNH1-GFP depends on transcription-replication interference and R-loop formation. Cells were treated with CPT (1 μM) or PDS (20 μM) for 5 h. Olaparib (PARPi, 10 μM), cordycepin (CORD; 50 μM) and aphidicolin (5 μM; APH), respectively, were added 2 h prior to CPT/PDS treatment as indicated. DNA breakage was monitored by pulsed-field gel electrophoresis (*top panels*) and quantified using Image-J software (*bottom panels*). Data were normalized and represent the mean ± S.D., n = 3. ****$P < 0.0001$ (Unpaired t-test). DSB, double-strand break. (B) Effect of depletion of the indicated proteins on the level of DNA

breakage in U2OS cells treated for 5 h with 1 μM CPT (black bars) or 10 μM PDS (grey bars) in the presence of PARPi. Genomic DNA was analyzed as in (A). Data represent the mean ± S.D., n = 4. (C) The level of DNA breakage in RA3331/E6E7/hTERT fibroblasts, complemented with either SLX4 wild type (WT) or SLX4 ΔSAP cDNAs, upon treatment with indicated concentrations of CPT. Genomic DNA was analyzed as in (A). Data represent the mean ± S.D., n = 4. (D) Effect of CPT (100 nM) and PDS (10 μM) on replication fork progression in cells in (C) prior to and after PARP inhibition. *Top panel*: Experimental workflow of DNA fiber assays. Where indicated, PARPi was added 2 h before CldU labeling. *Bottom panel*: Box plot of values of IdU/CldU tract length ratio obtained for indicated conditions in three independent experiments (n ≥ 200, whiskers: 10-90 percentiles). ns, not significant; ****P < 0.0001 (Mann-Whitney test). (E and F) Representative immunofluorescence images (G) and quantification (H) of MUS81 foci (green) colocalizing with FANCD2 foci (red) in U2OS cell nuclei (DAPI, blue) prior to and after treatment with PDS (10 μM) or CPT (100 nM) for 1 h. Data represent the mean ± S.D., n = 3. At least 100 cells were scored for each condition in each experiment. (G and H) Effects of RNase H1 (RNH1) overexpression and transcription inhibition with cordycepin (CORD) on the formation of FANCD2 (G) and MUS81 (H) foci in U2OS T-REx/RNH1-GFP cells treated with CPT (100 nM) or PDS (10 μM) for 1 h. RNH1-GFP expression was induced 24 h prior to CPT treatment. CORD (50 μM) was added 2 h prior to addition of CPT or PDS. Horizontal lines represent the mean ± S.E.M. At leased 300 cells were scored for each condition in three independent experiments. (I) Effect of SLX4 and EME1 depletion of the formation of FANCD2-positive MUS81 foci in U2OS cells treated with CPT for 1 h. Data represent the mean ± S.D., n = 3. At least 100 cells were scored for each condition in each experiment. Also see Figure S3.

Chappidi et al., Figure 4

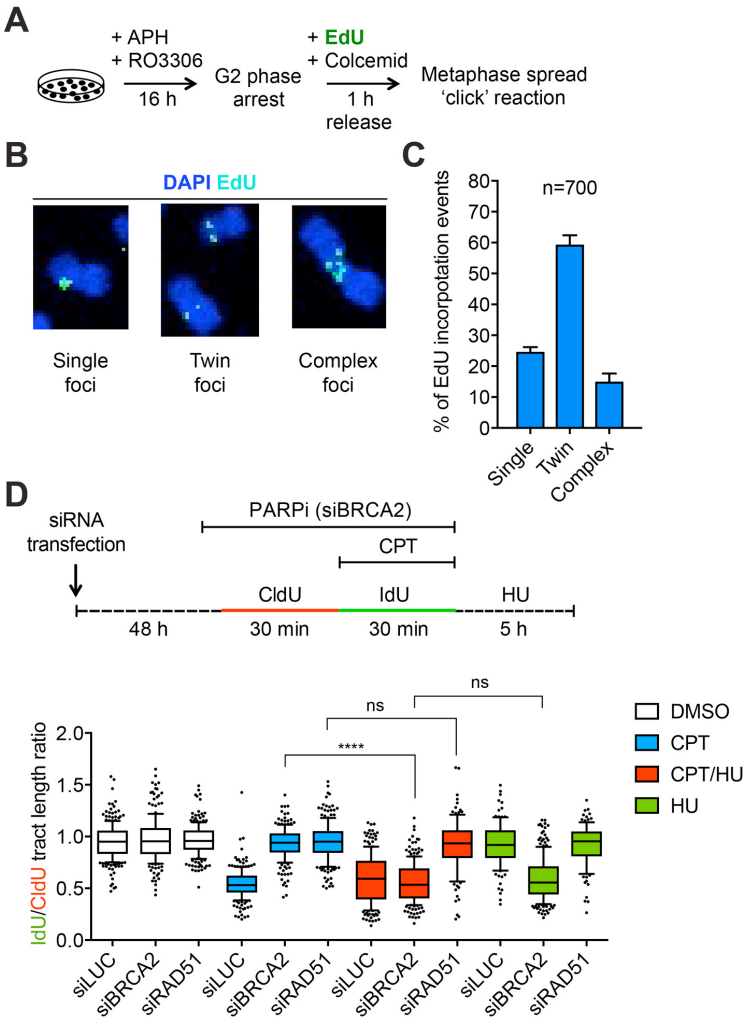

Figure 4. Preference for semiconservative mode of DNA replication following TRCs.
(A-C) Experimental work flow (A), representative images (B) and quantification (C) of EdU incorporation (cyan) on isolated metaphase chromosomes (DAPI, blue) following replication stress induced by low-dose of aphidicolin (+APH, 0.4 μM). Most sites of EdU incorporation exhibit a semiconservative pattern of DNA synthesis, having EdU incorporation on both sister chromatids, which appears as twin EdU foci. (D) Nascent DNA strands generated in BRCA2-deficient cells in the presence of CPT and PARPi are sensitive to degradation upon replication arrest by hydroxurea (HU). *Top panel*: Experimental workflow of DNA fiber assays. U2OS cells were transfected with indicated siRNA before CldU and IdU labelling (30 min for each pulse). Where indicated, cells were treated with CPT (100 nM) during IdU labeling and/or with HU (4 mM) for 5 h after IdU labeling. BRCA2-depleted cells were cultured in the presence of olaparib (PARPi; 10 μM) during DNA fiber labeling. *Bottom panel*: Box plot of values of IdU/CldU tract length ratio for mock (siLUC)-, BRCA2- and RAD51-depleted U2OS cells treated as indicated. At least 200 IdU/CldU tracts were measures for each condition in three independent experiments. Whiskers indicate 10-90 percentiles. ns, not significant; ****P < 0.0001 (Mann-Whitney test). Also see Figure S4.

Chappidi et al., Figure 5

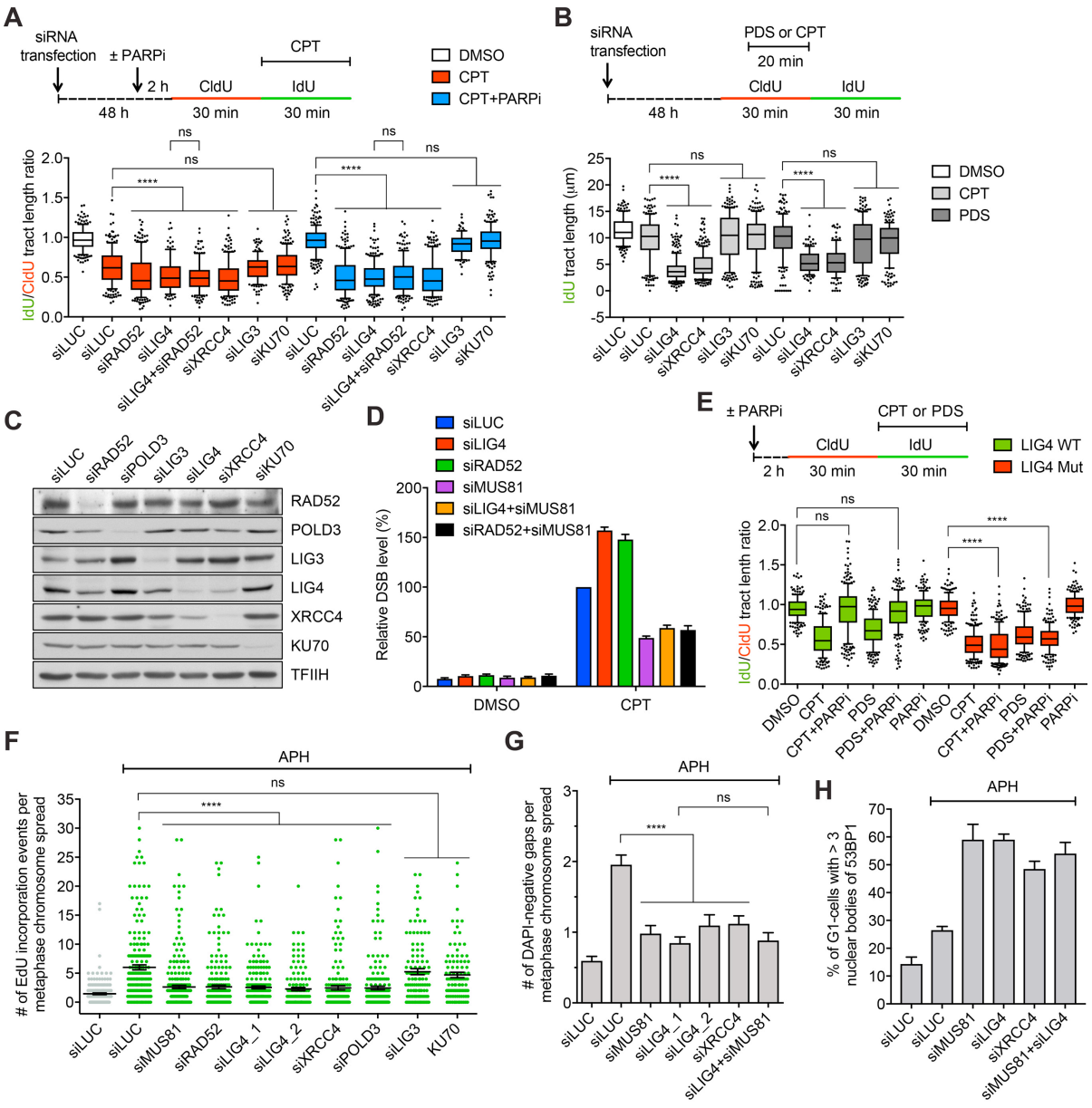

Figure 5. LIG4/XRCC4 complex is required for replication restart upon TRCs
(A) Effect of depletion of the indicated proteins on the replication fork velocity in U2OS cells upon treatment with 100 nM CPT, and on the rescue of CPT-induced replication fork slowing by PARP inhibition with 10 μM olaparib (PARPi). *Top panel*: Experimental workflow of DNA fiber assays. *Bottom panel*: Box plot of values of IdU/CldU tract length ratio obtained for indicated conditions in three independent experiments (n ≥ 200, whiskers: 10-90 percentiles). ns, not significant; ****P < 0.0001 (Mann-Whitney test). (B) Effect of depletion of the indicated proteins on replication fork velocity after treatment of U2OS cells with 100 nM CPT. *Top panel*: Experimental workflow of DNA fiber assay. *Bottom panel*: Box plot of values of IdU tract length obtained for indicated conditions in three independent experiments (n ≥ 200, whiskers: 10-90 percentiles). ns, not significant; ****P < 0.0001 (Mann-Whitney test). (C) Western blot analysis of extracts of U2OS cells transfected with indicated siRNAs. (D) The levels of spontaneous (DMSO) and CPT-induced DNA breakage in U2OS cells depleted for indicated proteins. Cells treated with 1 μM CPT for 5 h. Genomic DNA was

analyzed as in Figure 3A. Data represent the mean ± S.D., n = 4. (E) Effect of CPT or PDS on replication fork progression in human fibroblasts expressing wild-type (LIG4 WT, 1BR) or catalytically-inactive (LIG4 MUT, 411 BR) forms of LIG4, with or without PARP inhibition. DNA fiber assays were performed as in Figure 4D. (F) LIG4/XRCC4 is required for mitotic DNA synthesis in U2OS cells following replication stress induced by low-dose of APH (0.4 μM). MiDAS assay was performed as depicted in Figure S5B. Data points represent number of EdU incorporation events per metaphase spread. Horizontal lines represent the mean ± S.E.M. At least 150 metaphases were analyzed for each condition in three independent experiments. ns, not significant; ***P < 0.001; ****P < 0.0001 (Mann-Whitney test). (G) Quantification of DAPI-negative gaps on metaphase chromosome spreads of APH-treated U2OS cells depleted for indicated proteins. Data represent the mean ± S.E.M. At least 100 metaphases were scored for each condition in three independent experiments. ns, not significant; ****P < 0.0001 (Mann-Whitney test). (H) Quantification of G1-specific 53BP1 nuclear bodies in U2OS cells depleted for indicated proteins. Where indicated cells were treated with 0.4 μM APH for 16 h. Data represent the mean ± S.D., n =3. Also see Figure S5.

Chappidi et al., Figure 6

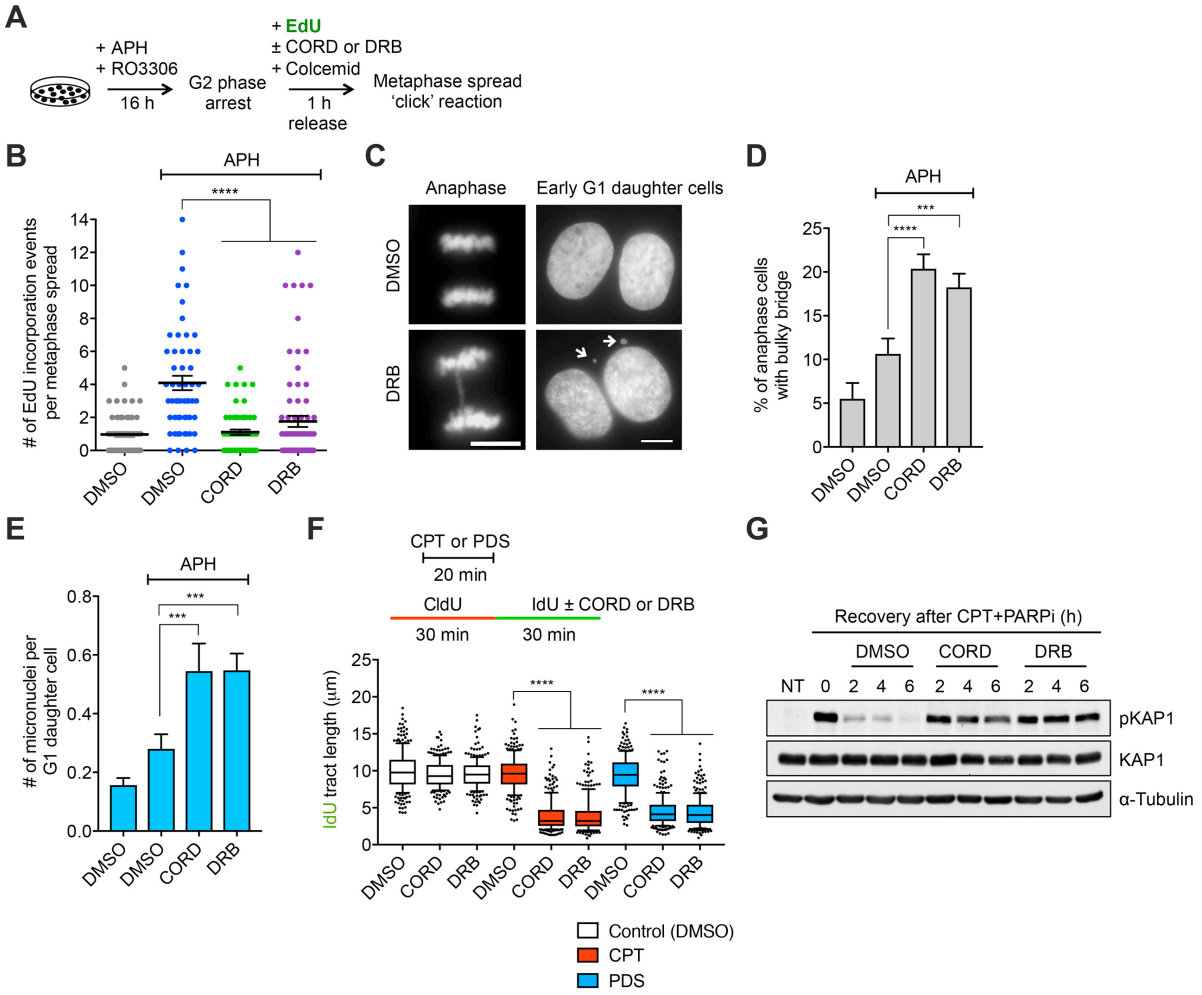

Figure 6. Replication restart upon R-loop-mediated TRCs requires active transcription
(A) Experimental workflow of MiDAS assay. (B) Effect of DRB (100 µM) or cordycepin (CORD, 50 µM) on EdU incorporation in U2OS cells released from G2 arrest following exposure to 0.4 µM aphidicolin (APH) as depicted in (A). Data represent the mean ± S.E.M.. At least 60 metaphases were analyzed for each condition in two independent experiments. ns, not significant; ****P < 0.0001 (Mann-Whitney test). (C) Examples of DAPI-stained anaphase bridges and micronuclei formed following release of APH-treated U2OS cells from G2 arrest in the presence of DRB. (D and E) Quantification of the frequency of anaphase bridges (D) and micronuclei (E) for cells treated as in (C). Data represent the mean ± S.D., n = 4. ***P < 0.001, ****P < 0.0001 (Unpaired t-test). (F) Effect of DRB or cordycepin of replication fork velocity in U2OS cells after treatment with 100 nM CPT or 10 µM PDS. *Top panel*: Experimental workflow of DNA fiber assays. *Bottom panel*: Box plot of values of IdU tract length measured for indicated conditions in three independent experiments (n ≥ 200, whiskers: 10-90 percentiles). ****P < 0.0001 (Mann-Whitney test). (G) Effect of DRB or cordycepin on the levels of KAP1 Ser824 phosphorylation (pKAP1) during the recovery of U2OS cells after 1-h treatment with 1 µM CPT and 10 µM olaparib (PARPi). Also see Figure S6.

Chappidi et al., Figure 7

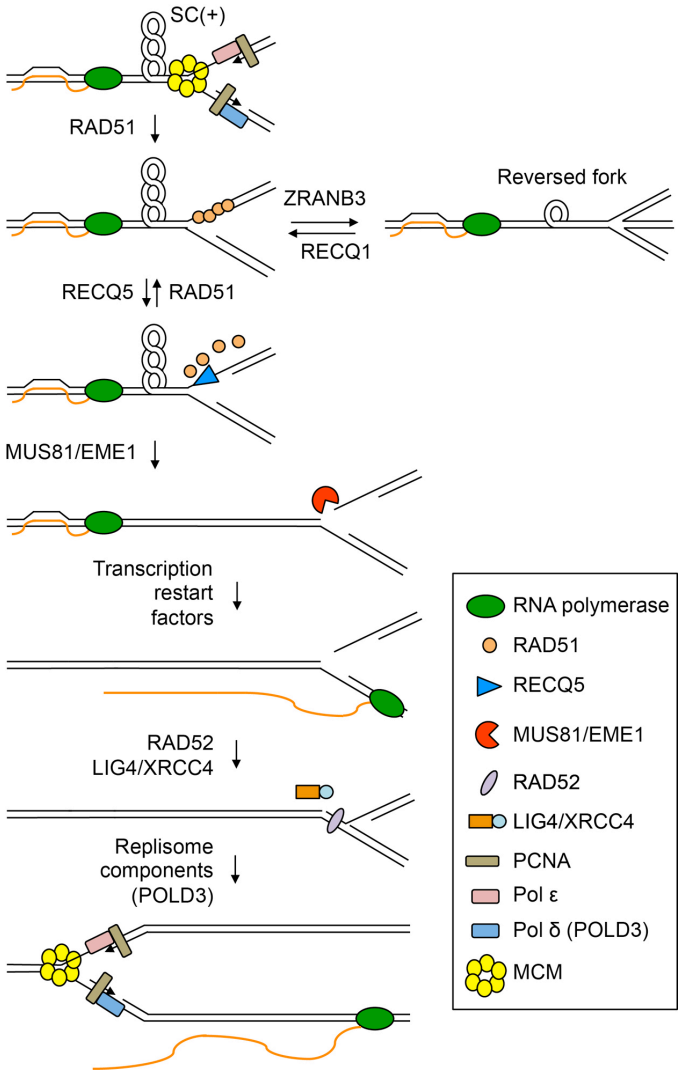

Figure 7. Model for resolution of R-loop-mediated TRCs
The blockage of replication forks by oncoming transcription complexes results from the build-up of positive supercoiling within the intervening DNA region and the formation of co-transcriptional R-loops. Replication fork stalling leads to the assembly of RAD51 filaments on the parental DNA strands at the fork junction, which promote fork reversal in conjunction with the DNA translocase ZRANB3. RECQ1 DNA helicase counteracts replication fork reversal to promote replication restart. In this pathway, RECQ5 DNA helicase disrupts RAD51 filaments to facilitate fork cleavage by MUS81/EME1 endonuclease. This relieves the topological barrier in the DNA template, allowing transcription restart. After RNA polymerase passage, replication fork is re-assembled by RAD52-mediated re-annealing of the parental strands and sealing the nick in the parental duplex by the LIG4/XRCC4 complex. This is followed by POLD3-dependent replisome reloading to reestablish semiconservative DNA replication.

SUPPLEMENTAL FIGURES

Chappidi et al., Figure S1

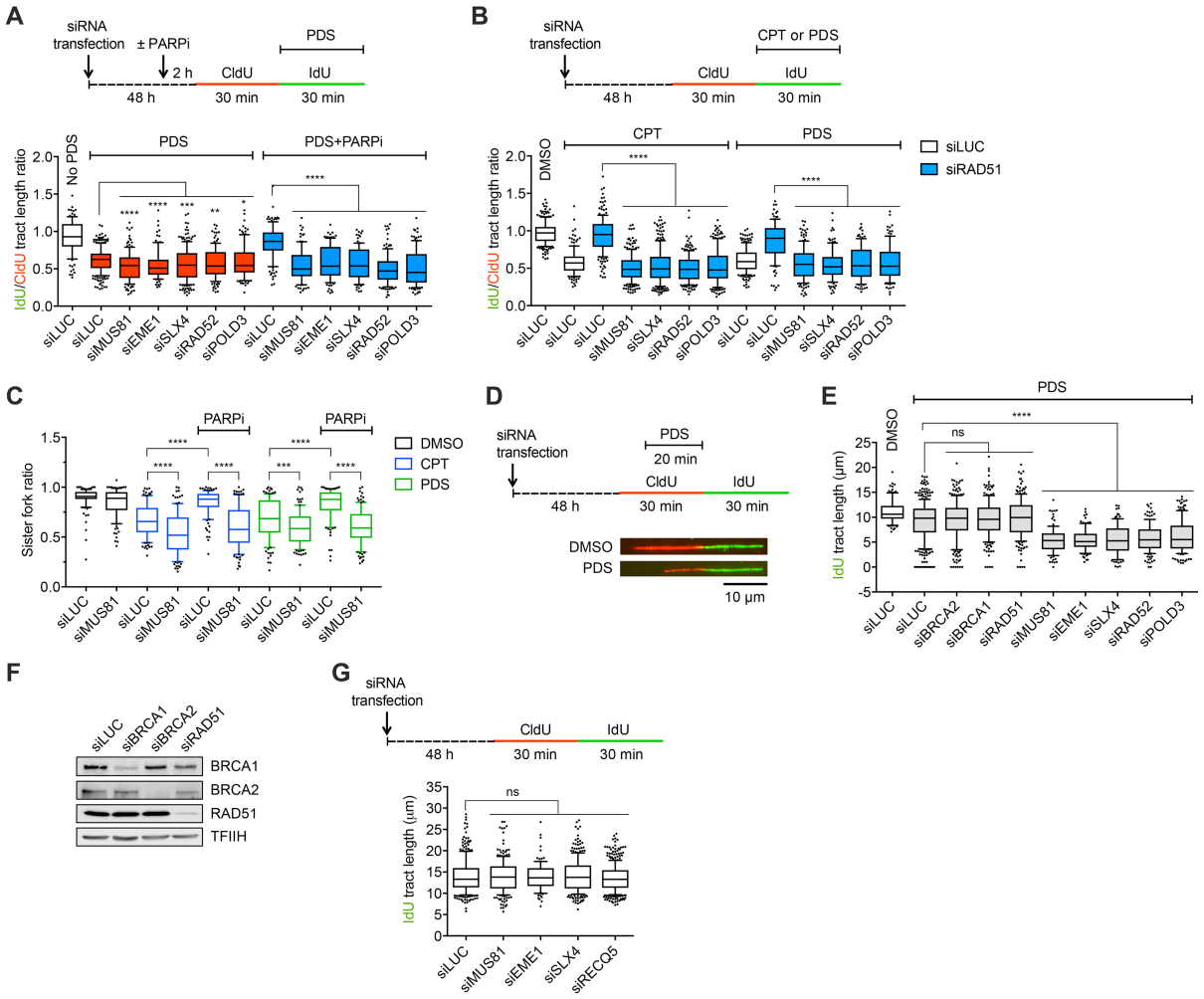

Figure S1, related to Figure 2.
(A) Effect of depletion of MUS81, EME1, SLX4, RAD52 and POLD3, respectively, on the replication fork velocity in U2OS cells upon treatment with 10 µM pyridostatin (PDS), and on the rescue of PDS-induced replication fork slowing by PARP inhibition with 10 µM olaparib (PARPi). *Top panel*: Experimental workflow of DNA fiber assays *Bottom panel*: Box plot of values of IdU/CldU tract length ratio obtained for indicated conditions in three independent experiments (n ≥ 200, whiskers: 10-90 percentiles). ns, not significant; *P = 0.0252, **P = 0.0022, ***P = 0.0004, ****P < 0.0001 (Mann-Whitney test). (B) Effect of depletion of MUS81, EME1, SLX4, RAD52 and POLD3, respectively, on the rescue of CPT- and PDS-induced replication fork slowing in U2OS cells by RAD51 depletion. *Top panel*: Experimental workflow of DNA fiber assays. *Bottom panel*: Box plot of values of IdU/CldU tract length ratio obtained for indicated conditions in three independent experiments (n ≥ 200, whiskers: 10-90 percentiles). ns, not significant; ****P < 0.0001 (Mann-Whitney test). (C) Effect of MUS81 depletion and PARP inhibition of replication fork asymmetry in U2OS cells treated with CPT or PDS. Images of DNA fibers from experiments in Figure 2A and

S1A were analyzed. Ratio of lengths of IdU tracts of sister forks is plotted for indicated conditions (n ≥ 100, whiskers: 10-90 percentiles). ****P < 0.0001 (Mann-Whitney test). (D) Experimental workflow of replication recovery assays and representative images of replication tracts detected on DNA fibers of mock-depleted (siLUC) U2OS cells upon indicated conditions. Cells were labeled sequentially with IdU and CldU for 30 min each. Where indicated, PDS (10 μM) or DMSO (mock treatment) were added during the last 20 min of the CldU pulse. (E) Effect of depletion of the indicated proteins on replication fork velocity in U2OS cells after their treatment with PDS. At least 200 IdU tracts were scored for each condition in three independent experiments. Whiskers indicate 10-90 percentiles. ns, not significant; ****P < 0.0001 (Mann-Whitney test). (F) Western blot analysis of extracts of U2OS cells transfected with indicated siRNAs. Cells were harvested 48 h post siRNA transfection. (G) Effect of depletion of MUS81, EME1, SLX4 and RECQ5, respectively, on replication fork velocity in unperturbed U2OS cells. *Top panel*: Experimental workflow of DNA fiber assay. *Bottom panel*: Box plot of values of IdU tract length obtained for indicated condition in three independent experiments (n ≥ 200, whiskers: 10-90 percentiles). ns, not significant (Mann-Whitney test).

Chappidi et al., Figure S2

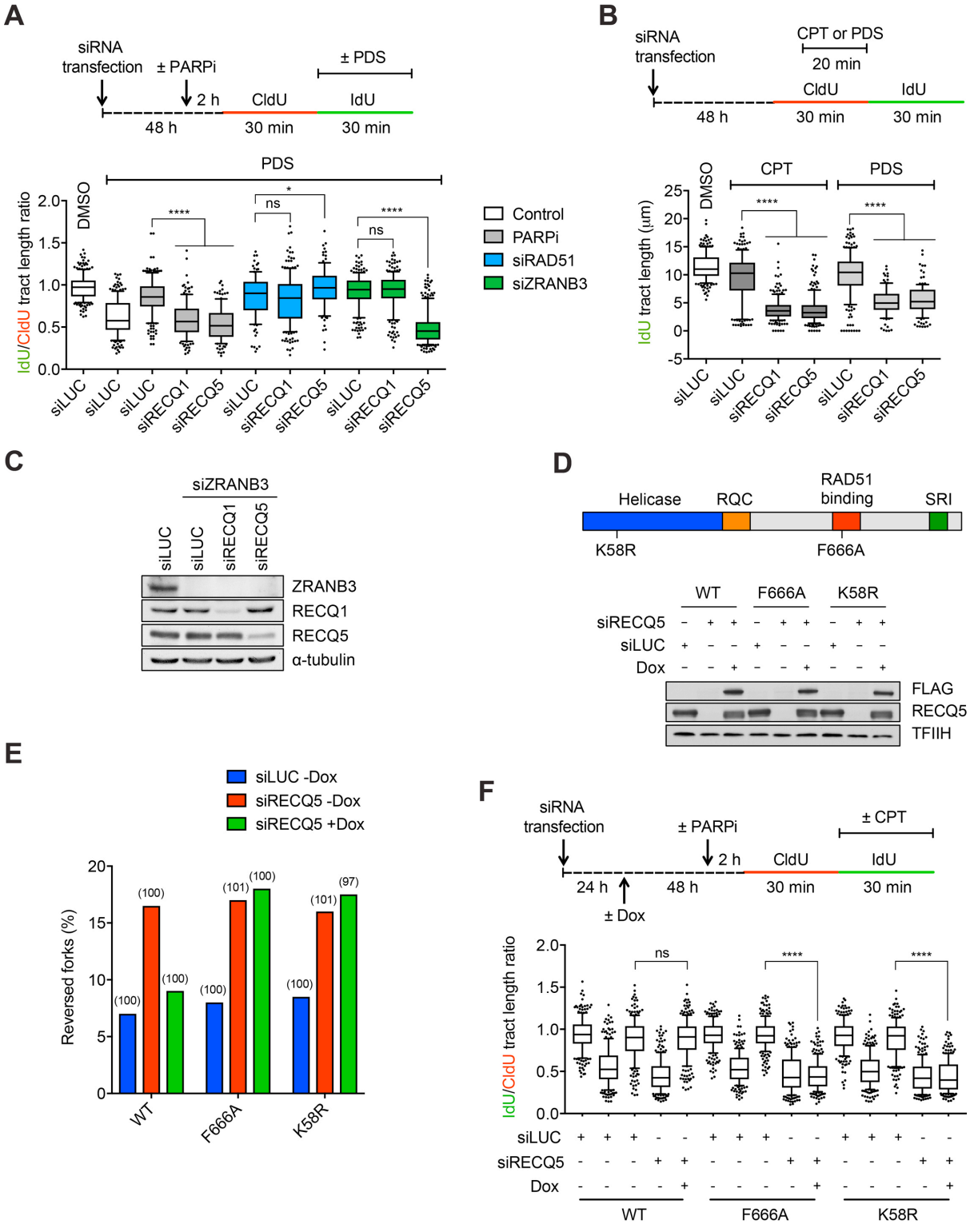

Figure S2, related to Figure 2.

(A) Effects of depletion of RECQ1 and RECQ5 on the rescue of replication fork slowing in PDS-treated U2OS cells by PARP inhibition (PARPi) and RAD51 or ZRANB3 depletion, respectively. *Top panel*: Experimental workflow of DNA fiber assays. *Bottom panel*: Box plot of values of IdU/CldU tract length ratio obtained for indicated conditions in three independent experiments ($n \geq 200$, whiskers: 10-90 percentiles). ns, not significant; *P = 0.0119; ****P < 0.0001 (Mann-Whitney test). (B) Effects of RECQ1 and RECQ5 depletion of replication fork velocity in U2OS cells after their treatment with CPT and PDS, respectively. *Top panel*: Experimental workflow of replication recovery assays. Cells were labeled sequentially with IdU and CldU for 30 min each. Where indicated, CPT (100 nM) or PDS (10 μM) were added during the last 20 min of the CldU pulse. *Bottom panel*: Box plot of values of IdU tract length obtained for indicated conditions in three independent experiments ($n \geq 200$, whiskers: 10-90 percentiles). ns, not significant; ****P < 0.0001 (Mann-Whitney test). (C) Western blot analysis of extracts of U2OS cells transfected with indicated siRNAs. Cells were harvested 48 h post siRNA transfection. (D) *Top panel:* Schematic representation of RECQ5 domain organization. RQC, RecQ C-terminal domain; KIX, kinase-inducible domain interacting; 51BD, RAD51-binding domain; SRI, Set2-Rpb1 Interaction motif. The location of K58R and F666A mutations is indicated. *Bottom panel:* Western blot analysis of extracts of U2OS T-REx cells harboring wild-type (WT), K58R or F666A forms of siRNA-resistant RECQ5-Flag fusion gene controlled by a doxycycline-inducible promoter. 24 h after transfection of indicated siRNAs, doxycycline (Dox, 0.4 ng/ml) or DMSO was added with fresh medium for a further 48 h as indicated. (E and F) Frequency of spontaneous replication fork reversal (E) and effect of PARPi on CPT-induced replication fork slowing (F) in cells in (D). Three conditions were analyzed for each cell line: siLUC -Dox (expression of endogenous RECQ5), siRECQ5 -Dox (RECQ5 depletion) and siRECQ5 +Dox (replacement of endogenous RECQ5 with RECQ5 variant). (E) The numbers in brackets indicate the number of analyzed molecules. Similar results were obtained in an independent experiment (Table S1C). (F) Box plot of values of IdU/CldU tract length ratio obtained for indicated conditions in three independent experiments ($n \geq 200$, whiskers: 10-90 percentiles). ns, not significant; ****P < 0.0001 (Mann-Whitney test).

Chappidi et al., Figure S3

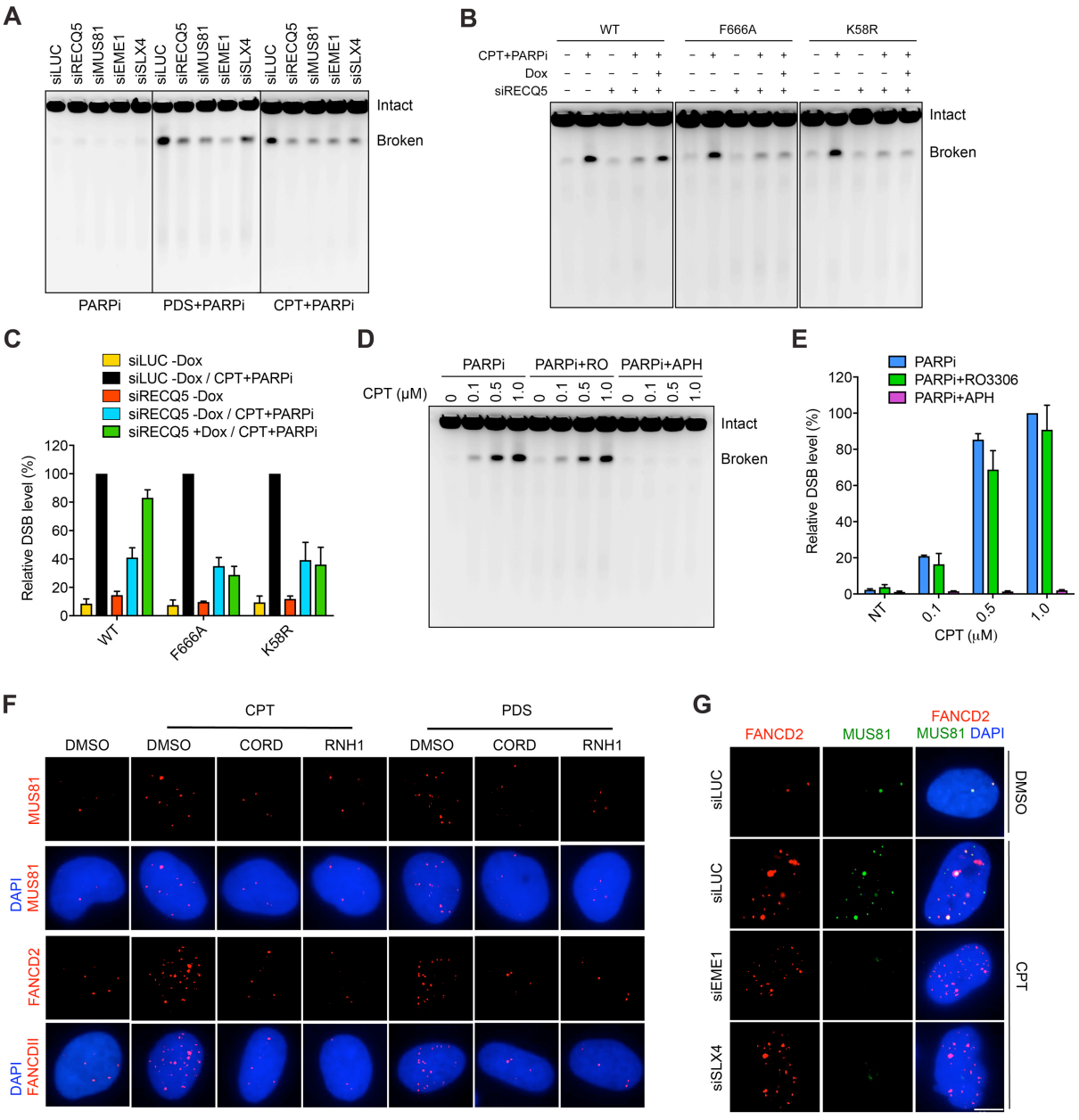

Figure S3, related to Figure 3.
(A) Pulsed-field gel electrophoresis analysis (PFGE) analysis of genomic DNA of U2OS cells treated with PARP inhibitor (PARPi) (*left panel*), PARPi + PDS (*middle panel*) and PARPi + CPT (*right panel*) at 48 h following transfection of the indicated siRNAs. PARPi. (10 μM) was added 2 h before addition of CPT (1 μM) or PDS (20 μM). CPT and PDS were present for 5 h. (B) The level of chromosomal DNA breakage in cells in (B) grown under indicated conditions. Where indicated, cells were treated with CPT (1 μM) and PARPi. (10 μM) for 5 h. Genomic DNA was analyzed by PFGE as in (A). (C) Quantification of gels represented in (B). DNA bands were quantified using Image-J software. Data were normalized and represent the mean ± S.D., n = 3. (D) Effect of aphidicolin (APH, 1 μM) and RO3306 (RO, 9 μM) on chromosome breakage in U2OS cells treated with 1 μM CPT upon

PARP inhibition. PARPi, APH and RO were added 2 h before addition of CPT, and CPT was present for 5 h. Genomic DNA was analyzed by PFGE as in (A). (E) Quantification of gels represented in (D). DNA bands were quantified using ImageJ software. Data were normalized and represent the mean ± S.D., n = 3. (F) Representative immunofluorescence images of U2OS T-REx/RNH1-GFP cells treated as in Figure 3G and 3H. Cells were stained for MUS81 (green) and FANCD2 (red). Nuclei were stained with DAPI (blue). (G) Representative immunofluorescence images of mock- (siLUC), SLX4- and EME1-depleted U2OS cells prior to (NT) and after treatment with CPT (100 nM) for 1 h. Cells were stained for MUS81 (green) and FANCD2 (red). Nuclei were stained with DAPI (blue).

Chappidi et al., Figure S4

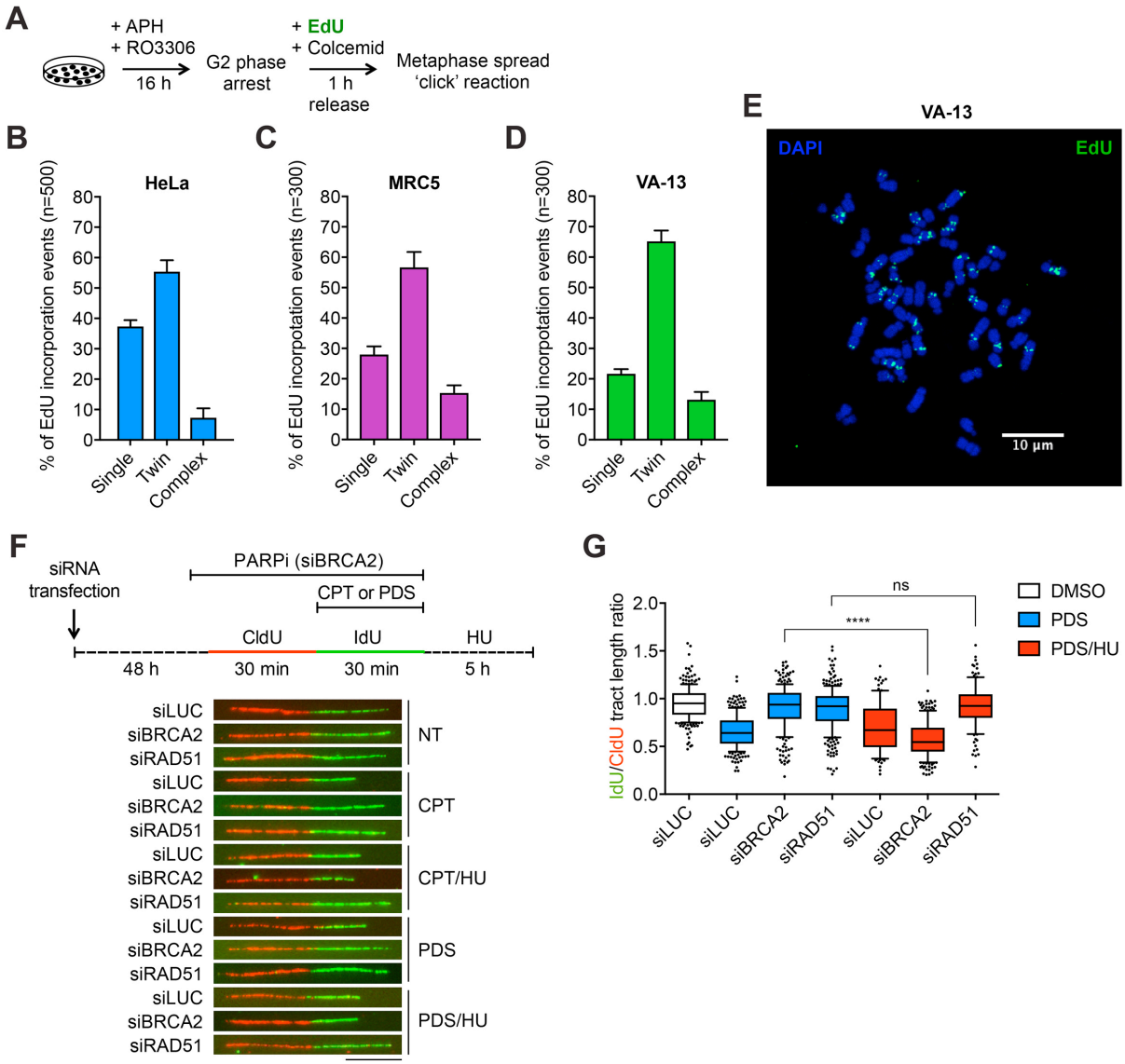

Figure S4, related to Figure 4.
(A-D) Experimental work flow (A) and quantification of EdU incorporation on metaphase chromosome spreads of HeLa (B), MRC5 (C) and VA-13 (D) cells following replication stress induced by low-dose of aphidicolin (+APH, 0.4 µM). Twin EdU foci (one on each sister chromatid) indicate semiconservative DNA replication. RO3306 was present at a concentration of 9 µM. (E) Representative image of EdU foci on metaphase chromosome spread of VA-13 cells treated as depicted in (A). (F) Experimental workflow of DNA fiber assays and representative images of replication tracts detected on DNA fiber spreads of U2OS cells treated as indicated. U2OS cells were transfected with indicated siRNA before CldU and IdU labeling (30 min for each pulse). Where indicated, cells were treated with CPT (100 nM) or PDS (10 µM) during IdU labeling, and/or with HU (4 mM) for 5 h after IdU labeling. BRCA2-depleted cells were cultured in the presence of olaparib (PARPi, 10 µM) during DNA fiber labeling. NT, non-treated. Scale bar, 10 µm. (G) Nascent DNA strands generated in BRCA2-defective cells in the presence of PDS and PARPi are sensitive to degradation upon replication arrest by HU. Box plot representation of values of IdU/CldU

tract length ratio for mock (siLUC)-, BRCA2- and RAD51-depleted U2OS cells treated as indicated. At least 200 IdU/CldU tracts were measures for each condition in three independent experiments. Whiskers indicate 10-90 percentiles. ns, not significant; ****P < 0.0001 (Mann-Whitney test).

Chappidi et al., Figure S5

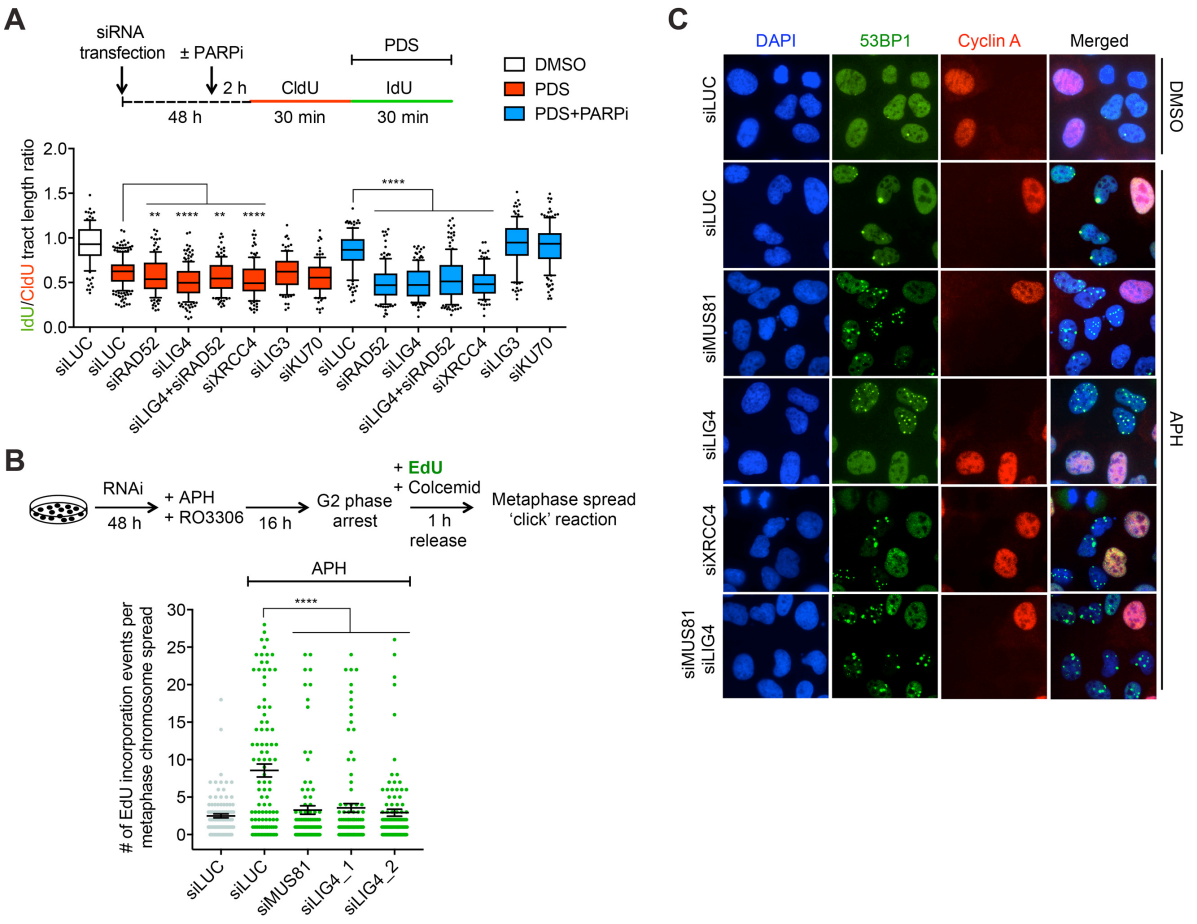

Figure S5, related to Figure 5.
(A) Effect of depletion of the indicated proteins on the replication fork velocity in U2OS cells upon treatment with 10 µM PDS, and on the rescue of PDS-induced replication fork slowing by PARP inhibition with 10 µM olaparib (PARPi). *Top panel*: Experimental workflow of DNA fiber assays. *Bottom panel*: Box plot of values of IdU/CldU tract length ratio obtained for indicated conditions in three independent experiments (n ≥ 200, whiskers: 10-90 percentiles). **P = 0.0022; ***P = 0.001; ****P < 0.0001 (Mann-Whitney test). (B) LIG4/XRCC4 is required for mitotic DNA synthesis (MiDAS) in SV40-immortalized MRC5 fibroblasts following replication stress induced by low-dose of aphidicolin (APH). *Top panel*: Experimental workflow of MiDAS assay. 48 h after siRNA transfection, cells were treated with APH (0.4 µM) and RO-3306 (9 µM) for 16 h (late G2 arrest), and then released into fresh medium containing EdU (20 µM) and colcemid (0.1 µg/ml) for a further 1 h. Metaphase chromosome spreads we subjected to click reactions to visualize the sites of EdU incorporation. *Bottom panel*: Quantification of EdU foci on metaphase spreads for cells transfected with indicated siRNAs. Twin or complex EdU foci were counted as one event. Horizontal lines represent the mean ± S.E.M. At least 100 metaphases were analyzed for each condition in three independent experiments. ****P < 0.0001 (Mann-Whitney test). (C) Examples of G1 phase U2OS cells (cyclin A-negative, red) containing 53BP1 nuclear bodies (green). Where indicated, cells were depleted of MUS81, LIG4, and XRCC4, and treated with 0.4 µM APH for 16 h.

Chappidi et al., Figure S6

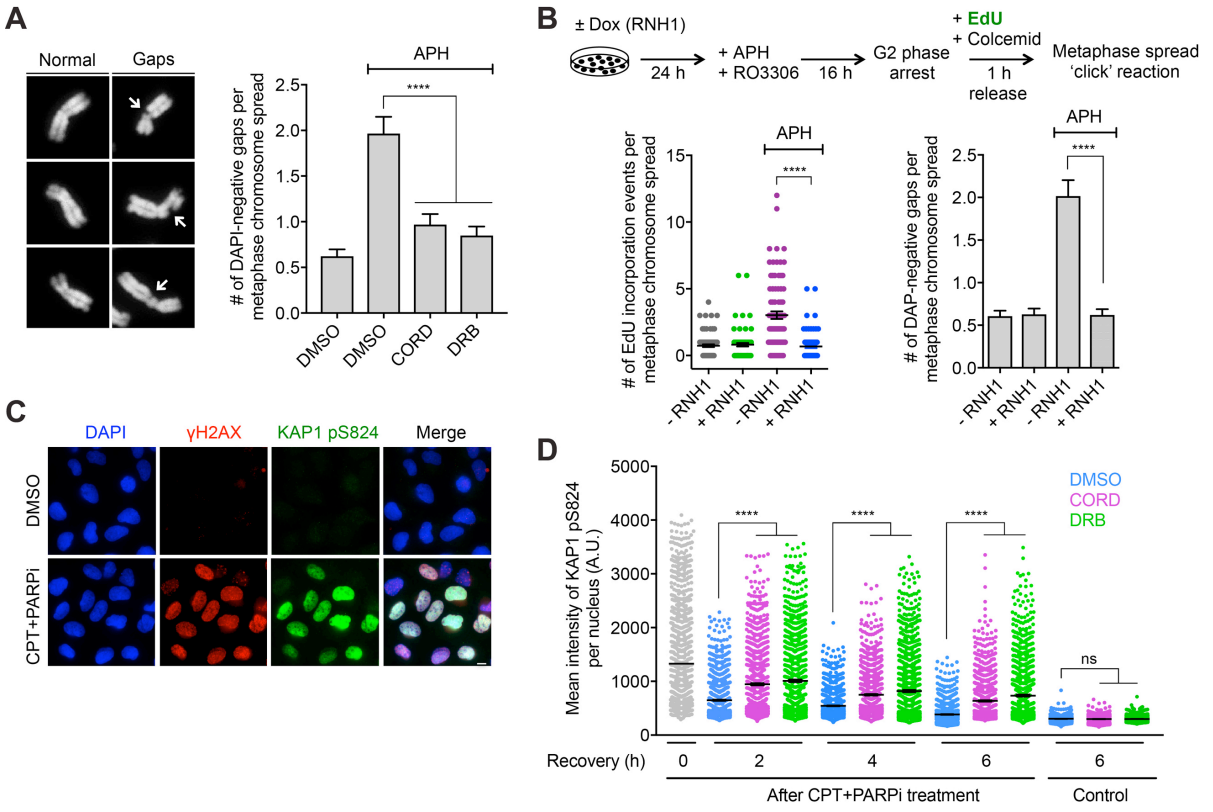

Figure S6, related to Figure 6.
(A) Expression of common fragile sites is impaired by inhibition of transcription during early mitosis. *Left panel*: Examples of metaphase chromosomes of U2OS cells treated with aphidicolin (APH) as depicted in Figure 6A. Arrows denote DAPI-negative gaps. *Right panel*: Quantification of DAPI-negative gaps on metaphase chromosome spreads of U2OS cells released from G2 arrest following exposure to 0.4 μM APH as depicted in Figure 6A. Where indicated, cells were released in the presence of DRB (100 μM) or cordycepin (CORD, 50 μM). DMSO was used as control. Data represent the mean ± S.E.M. At least 120 metaphases were analyzed in three independent experiments. (B) Mitotic DNA synthesis depends on R-loop formation. *Top panel:* Experimental workflow of mitotic DNA synthesis (MiDAS) assays. U2OS T-REx/RNH1-GFP cells were treated with 0.4 μM aphidicolin (APH) and 9 μM RO-3306 for 16 h (late G2 arrest), and then released into fresh medium containing EdU (20 μM) and colcemid (0.1 μg/ml) for a further 1 h. Where required, doxycycline (Dox, 1 ng/ml) was added to induce RNH1-GFP expression. *Bottom left panel:* Quantification of EdU incorporation on metaphase chromosomes of U2OS T-REx/RNH1-GFP cells grown under indicated conditions. For each condition, at least 150 metaphases from three independent experiments were analyzed. The graph is scattered dot plot with black lines at mean. Error bars show S.E.M. ****$P < 0.0001$ (Mann-Whitney test). *Bottom right panel:* Quantification of DAPI-negative gaps on metaphase chromosomes of U2OS T-REx/RNH1-GFP cells grown under indicated conditions. At least 110 metaphase spreads from three independent experiments were scored for each condition. Data are mean ± S.E.M. (C) Representative images of U2OS cells immunostained for γ-H2AX (red) and phospho-KAP1 pS824 (green) after treatment with CPT (1 μM) and PARPi (10 μM) for 1 h. For control, cells were mock treated with identical volume of DMSO. Nuclei were stained with

DAPI (blue). (D) Quantification of mean intensity of KAP1 pS824 fluorescence per nucleus in arbitrary units (A.U.). U2OS cell were treated with CPT and PARPi as in (C), and then released in to the fresh medium containing either DRB (100 μM) or CORD (50 μM). For control, DMSO was used. Cells were collected at indicated time points and immunostained as in (C). Mean intensity of KAP1 pS824 fluorescence was quantified using ImageJ. For each condition, at least 1000 nuclei from three independent experiments were analysed. The graph is scattered dot plot with black lines at mean. Error bar show SEM. ns, not significant; ****$P<0.0001$ (Mann-Whitney test).